Parameterization of a Non-Linear Groundwater Storage-Discharge Relationship for PCR-GLOBWB

Universiteit Utrecht

Master's Thesis – MSc Water Science and Management

Muhammad Arfan

Supervisors: Prof. dr. ir. Marc Bierkens, Dr. ir. Edwin H. Sutanudjaja

2nd Assessor: Dr. ir. Niko Wanders

Word count: 7799

14th July 2024

Table of Contents

List of Figures

Abstract

Groundwater is an essensial major water resource that is utilized for human water needs and is an integral part of the intricate water system. To grasp its complexity and challenges, a global groundwater model has been developed. This model predicts future groundwater patterns, especially under the influence of climate change, and serves as a risk mitigation tool in groundwater management.

PCR-GLOBWB 2 is one such global hydrological model that can be coupled with the groundwater model. In this groundwater model, the linear reservoir concept is applied. However, some previous studies have indicated a non-linear relationship between baseflow and groundwater storage represents a better reality compared to the linear reservoir. Therefore, we aim to identify and apply this non-linearity using the recent groundwater model, GLOBGM. Additionally, we explore the multiple drainages and various conductance concepts to explore potential model improvements.

The result of this recent advancement concept does not yet show an entire improvement. However, improvements are observed partially, especially in regions with wet or high-precipitation climates based on their Kling-Gupta Efficiency (KGE) values. In contrast, the model performs poorly in most dry climate areas, sometimes failing to simulate discharge, as seen in the River Niger, Mali, where it only shows a zero value for some periods.

A very low variability and bias in the simulated data indicate that the discharge from the new model is still often underestimated when compared to observational GRDC data. The temporal dynamic of this new model, however, is better than the PCR-GLOBWB default version, as indicated by the correlation and determination coefficient (R^2), which shows a notable improvement.

In subsequent research, a novel regression approach may be taken into consideration to improve model performance. The very low recession coefficient found in this study can be replaced with the default recession coefficient from the PCR-GLOBWB 2 dataset to find a new baseflow exponent.

1. Introduction

Groundwater is an important water resource, containing about 30% of freshwater available on the earth, while the other 69% is locked in the form of ice (Galodha et al., 2023). It is utilized by billions of people for agriculture, drinking water, and industrial use (West et al., 2023). It also has a vital role in maintaining the integrity of groundwater-dependent ecosystems such as rivers, lakes, and wetlands (Li et al., 2019). Furthermore, groundwater is considered less influenced by external factors, rather than surface water (Mahammad et al., 2023). Hence, groundwater is a more reliable water resource than surface water, especially during droughts, when it contributes to springs and shallow wells as the remaining accessible water resources to use (Tallaksen and van Lanen 2004; Aeschbach-Hertig and Gleeson 2012; Taylor et al. 2013, Wada, 2015)

Groundwater monitoring and modeling play important roles in mitigating risks associated with groundwater management. Integrating a global groundwater model into a hydrological framework is essential for gaining a comprehensive understanding of the global water cycle dynamics, as emphasized by Condon et al. (2021). Moreover, the implementation of a global monitoring system is necessary to provide temporal groundwater data, serving as the cornerstone for robust global groundwater models. These models enable comprehensive analyses of the impacts of large-scale phenomena such as droughts and groundwater extraction on global groundwater resources. Recent advancements have yielded notable global groundwater models, including a high-resolution global-scale groundwater model (de Graaf et al., 2015), a global groundwater table depth model by Fan et al. (2013), and the Global Gradient-based Groundwater Model (G3m) developed by Reinecke et al. (2018)

One example of a global hydrological model which can be coupled with a groundwater model is PCR-GLOBWB. The groundwater model based on MODFLOW (Harbaugh et al., 2000) in PCR-GLOBWB simulated as a single linear reservoir per model grid cell considering a single drainage elevation, assuming a linear storage relationship:

$$Q_{gw} = \alpha S \qquad (1)$$

With:
Qgw = Baseflow
S = Storage
α = Relationship factor (storage coefficient)

The parameter alpha in this relationship, which essentially signifies a recession coefficient, is typically derived from drainage theory (e.g., Kraaijenhoof van de Leur, 1958) or calibration. Nonetheless, certain studies posit that linear reservoirs may not faithfully represent reality. In his research, Wittenberg (1999) argued that there is a strong non-linearity indication where the k value fitted in the semi-logarithmic plots of flow recession is mostly not constant, but systematically increases when the flow decreases. Furthermore, the assumption that the baseflow comes from two or more

parallel linea reservoirs (Moore 1997; Schwarze et al., 1997) is unlikely to occur because, in most areas, it is not common for the unconfined aquifer to be divided into independent storage zones, but is more rational owing to the interaction and exchange facilitated through the system of pores or fissure systems. Wittenberg (1999) introduces a new non-linear storage-discharge relationship:

$$S = aQ^{b} \quad (2)$$

$$Q = \left(\frac{S}{a}\right)^{\frac{1}{b}} \quad (3)$$

He posited that this correlation demonstrates a strong fit across a wide spectrum of discharge values in Germany, with the exponent b typically clustering around 2. His other research (Wittenberg, 1994) found that a similar value occurs in most rivers in China. He said that consistent findings were reported in studies by Drogue (1972) Werner and Sundquist (1951), Schoeller (1962), Rocher (1963), and Fukushima (1988), indicating that for discharge from springs and unconfined aquifers, the dimensionless constant b tends to hover around 2 (Wittenberg, 1999). However, the value of the b parameter can vary depending on the characteristics of the catchment area. Gan and Luo (2013) conducted a study discovering that the non-linear aquifer storage-discharge approach performs comparably to the traditional linear reservoir approach, with b values ranging from 1.00 to 5.0 and a mean value of 3.125. In a separate study focusing on a catchment area in the eastern part of Australia, Chapman (1999) found b values fluctuating between 1.64 and 3.23 instead of 1, indicating a non-linear relationship between groundwater storage and baseflow. Notably, a smaller b parameter signifies a higher discharge's sensitivity to groundwater storage (Chapman, 1999). A study (Moore,1996) indicates a similar result that the recession analysis between outflow and storage is more likely a non-linear form rather than a linear regression in a small forested catchment, in which most baseflow is contributed from the drainage of saturated groundwater storage in the shallow soil.

Hence, we endeavor to integrate the non-linear reservoir concept into PCR-GLOBWB, which previously relied on a linear reservoir model. With greater groundwater storage, water tables become shallower, leading to increased utilization of surface water systems. Consequently, groundwater discharge becomes more efficient with larger groundwater storage. This implies that the storage-discharge relationship should exhibit non-linearity. To investigate this, our study will examine various drainage elevations within the model.

$$Q_{gw} = \alpha S^{\beta} \quad (4)$$

To know whether the relationship is linear or not, we should find the value of β. The relationship is nonlinear if the β value is not equal to one. Since we need to find the β value for each grid on a global scale, the use of the current global groundwater model

of PCR-GLOBWB-MODFLOW will require high memory usage, data storage, and heavy run time. As the solution to this challenge, we use GLOBGM, which was developed by (Verkaik et al., 2024) which makes it possible to run the groundwater model on the global scale in a more efficient way.

In the current PCR-GLOBWB-MODFLOW groundwater model, the water from storage is only discharged from a single drainage. This single drainage is assumed equal to the floodplain. Consequently, the storage release of water to the stream is not proportional to what occurs in reality, especially in conditions where the storage level is getting higher or fluctuating. This problem can be solved by implementing multiple drainages in the groundwater storage. Since the GLOBGM can simulate the groundwater head on a global scale, it is applicable to implement the multiple drainages concept. With this new model, water from storage can be discharged from more than one drainage if the groundwater level is higher. However, this concept might be not representative and lead to the misvalue of the baseflow in a certain area. For instance, the baseflow in the area with low elevation would be very sensitive to the amount of drainages applied. Hence, we implemented various conductances for each elevation to prevent that condition occurs.

2. Research questions

The main objective of this research is to derive and parameterize an improved non-linear storage-outflow relationship for global hydrological models of PCR-GLOBWB. This study also will exercise how the current development of GLOBGM is implemented in simulating the groundwater head on a global scale with multiple drainages and various conductance concepts, and whether it will lead to a better simulation of the discharge, compared to the simulation with the previous PCR-GLOBWB groundwater model. Hence, a research question is raised:

"Can we improve PCR-GLOBWB performance with the new nonlinear storage-outflow relationship?"

To help answer this research question properly, some sub-research questions are arranged:

1. Can the new relationship capture the non-linearity between the storage and baseflow using the GLOBGM?
2. What is the new model's performance in simulating discharge based on the Kling-Gupta Efficiency (KGE) indicators?
3. In which areas does the model demonstrate improved performance?
4. Which component of the KGE has been improved by the new model?

We will answer this question by using the GLOBGM, a recent development in 30 arcsec resolution. The output of this simulation later will be an input of the PCR-GLOBWB to simulated discharge. Furthermore, this discharge will be compared to the GRDC observation discharge, and the performance of the model will be evaluated by the Kling-Gupta efficiency (KGE) indicators. Due to the heavy computation and high

memory usage, we will use the Dutch national supercomputer Snellius to simulate the model. The detailed method of the research will be explained in the section 3.

3. Material and methods

3.1 General approach

This study consists of two models, the first is the groundwater model GLOBGM v1.0 at 30'' resolution, and the second is a hydrological model PCR-GLOBWB 2 that will be run in the resolutions of 5'.

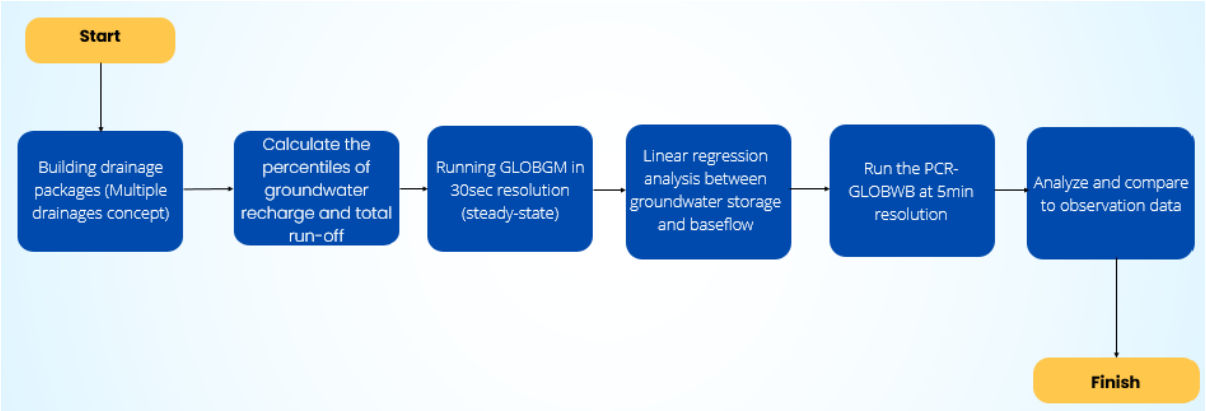

Figure 1 A workflow for this research

The research was started by applying the multiple drainages and conductance concept to the current MODFLOW drainage package. Furthermore, eleven scenarios were created based on the variation of groundwater recharge and total run-off. We ran the GLOBGM multiple times based on the number of scenarios we had and it simulated eleven groundwater heads. This groundwater head will be used to calculate the baseflow and groundwater storage. After that, we performed a linear regression to this baseflow and storage based on the newly developed baseflow-storage formula. The output of linear regression is used as an input in running the PCR-GLOBGM to simulate the discharge. For the last step, we analyzed the simulated discharge to the GRDC observation discharge to see the improvement of the new model. The next section will provide a detailed explanation of the method and how we use the model.

3.2 GLOBGM

3.2.1 General description

GLOBGM is a further development of 5 arcminutes (10 km at the equator) of the PCR-GLOBWB 2 MODLFOW-based global two-layer groundwater model that simulates the model at 30 arcseconds or 1 km at the equator (Verkaik et al., 2024). The development into finer resolutions makes GLOBGM have more cells than the PCR-GLOBWB-MODFLOW groundwater model. It means the simulation for this resolution requires a heavier runtime, memory usage, and storage (Verkaik et al., 2024). According to (Verkaik et al., 2024), GLOBGM can solve those computation problems by utilizing MODFLOW 6 to construct independent unstructured grids with a total of 278 million

active cells which reduces the redundancy of cells and distributed it into four groundwater models which are Afro-Eurasia, the Americas, Australia, and islands. This model will be partitioned as multiple non-overlapping sub-models which allow the simulation of the groundwater model in the global area in a parallel way. It leads to a more efficient simulation that reduces the run time of the simulation from ~4.5 months to only a maximum of 16 hours.

Based on (Verkaik et al., 2024), there are five steps, including the post-processing step in running the GLOBGM with the MODFLOW 6 version. The first step of the GLOBGM workflow is writing the tiles parameter. In this step, we prepare all the parameters that are needed within the tiles. The parameter data is inputted in the 30 arcsec resolution. The next step is to prepare model partitioning. In this step, it creates all necessary mapping that is used for the running process. Furthermore, the output of the previous two steps will be input in the next step called "Partition and Write Model Input". This step consists of three processes, which are "Area-Based Graph Partitioning", "Assemble & Write Submodel Input Data", and "Assemble & Write Inter-Submodel Connections" (Verkaik et al., 2024). After all the processes are completed, we can run the model in the "Run Model" step. In this step, the model will be run on a distributed memory parallel computer. The last step is "Post-Processing" which gives the output of groundwater head and water table depth for the top and bottom layers.

3.2.2 Developing multiple drainage packages for GLOBGM

In this research, we expand the model by developing the multiple drainages concept in the MODFLOW drainage package. The objective of this concept is to allow the model to have more active drainage if the groundwater level is higher. The system will have more water released through the drainage when it has more groundwater level. We developed two versions of MODFLOW drainage packages: (1) multiple drainage packages with a single conductance and (2) multiple drainage packages with various conductances. This development was conducted by modifying the MODFLOW drainage package. For the multiple drainage package with a single conductance, the equation that was used in the MODFLOW drainage packages is as follows:

$$Q_{drain} = \sum[c\ x \max(0, GH - drain\_elevation_i)] \quad (5)$$

$$c = Sy\ x\ cell\ area\ x\ \pi^2\ x \frac{KD}{Sy\ x\ L^2} \quad (6)$$

With:
GH = groundwater head (m)
K = Hydraulic conductivity (m/day)
c = drain conductances (m^2d^{-1})
D = aquifer thickness, with the assumption of 100 meters.
Sy = Specific yield (-)
L = Average distance between streams and rivers (m)

However, the equation above will cause the baseflow to be sensitive to the number of drainages, especially in the area with a small elevation variability. Hence, it can cause the model to overestimate the water discharged. To tackle this risk, we apply different conductances for each drainage elevation as the following equations:

$$c_i = Sy\ x\ cell\ area\ x\ \pi^2\ x \frac{KD_i}{Sy\ x\ L^2} \quad (7)$$

$$D_i = \text{elevation}_\text{i} - \text{elevation}_{\text{i}-1} \quad (8)$$

$$Q_{drain} = \sum[c_i\ x\ \max(0, GH - drain\_elevation_i)] \quad (9)$$

Where i is the number of drainage elevations, in this study we have 13 drainage elevations by calculating the elevation with fraction factors (0, 0.01, 0.05, 0.1, 0.2, 0.3, 0.4, 0.5, 0.6, 0.7, 0.8, 0.9, 1.0). Additionally, it should be noted that for Eq. (5) and Eq. (9), the drainage will be zero if the groundwater head is lower than the drainage elevation.

The aquifer thickness will be different in the various conductance concepts based on the drainage elevation. The lowest elevation or when i is equal to 1 is the floodplain. The assumption of the floodplain is 100 meters. So, the Eq. (7), (8), and (9) will be used only for i greater than 1.

3.2.3 GLOBGM runs

These two multiple drainage settings will be implemented for a steady-state simulation of the GLOBGM, where there was no groundwater abstraction is assumed (Verkaik et al., 2024). It ran in the tested areas such as Rhine-Meuse and Florida to see how are the differences between these set-ups, especially in low elevation areas before simulating it on a global scale. Furthermore, to see whether the baseflow and storage relationship is linear or not, we did a linear regression between the baseflow and storage, and to do that, various baseflow and groundwater storage data are needed. These various baseflow and storage are calculated by simulating GLOBGM with different scenarios.
The parameters that were modified in this simulation were groundwater recharge and total run-off. We used the groundwater recharge and total run-off from the HYPFLOWSCI6 (Hydrological Projection of Future Global Water States with CMIP6) historical dataset from 1979-2019. The various scenarios were created by determining the maximum, minimum, and percentiles (0.1, 0.2, 0.3, 0.4, 0.5, 0.6, 0.7, 0.8, and 0.9) of the groundwater recharge and total run-off. In total, we have 13 scenarios for this research.

The results of this simulation were eleven groundwater heads of the top and bottom layers. The top layer represents a confined aquifer, while the bottom layer is a confined aquifer. The model will treated as an unconfined aquifer if the confining layer is not present (de Graaf et al., 2017; Verkaik et al., 2024). We used the groundwater

head output to calculate the baseflow and groundwater storage. Baseflow is calculated as the sum of the river flux and drainage flux divided by cell area:

$$\text{Baseflow} = \frac{\text{river\_flux} + \text{drain\_flux}}{\text{Cell Area}} \quad (10)$$

The river flux (Q_{river}) is calculated by the following equations:

$$\mathrm{Q}_{\mathrm{river}_{\mathrm{top}}} = \begin{cases} RBC\ x\ \max(0, RSE - GH_{top}), & \text{if } GH_{top} > RBE \\ RBC\ x\ \max(0, RSE - RBE), & \text{if } GH_{top} < RBE \end{cases} \quad (11)$$

$$Q_{river_{bot}} = \begin{cases} RBC\ x\ \max(0, RSE - GH_{bot}), & \text{if } GH_{bot} > RBE \\ RBC\ x\ \max(0, RSE - RBE), & \text{if } GH_{bot} < RBE \end{cases} \quad (12)$$

$$\mathrm{Q}_{\mathrm{river}} = \mathrm{Q}_{\mathrm{river}_{\mathrm{top}}} + \mathrm{Q}_{\mathrm{river}_{bot}} \quad (13)$$

Where:
RSE = River stage elevation (m)
RBE = River bed elevation (m
RBC = River bed conductance (m)
GH_{top} = Groundwater head of top layer (m)
GH_{bot} = Groundwater head of bottom layer (m)

Furthermore, the drainage flux (Q_{drain}) was calculated by summing the drainage flux in the top layer ($\mathrm{Q}_{drain_{top}}$) and drainage flux in the bottom layer ($Q_{drain_{bot}}$), as given the following equations:

$$\mathrm{Q}_{drain_{top}} = \sum \mathrm{c_i}\ \mathrm{x}\ \ \max(0, GH_{top} - DEU_i) \quad (14)$$

$$Q_{drain_{bot}} = \sum \mathrm{c_i}\ \mathrm{x}\ \ \max(0, GH_{bot} - DEL_i) \quad (15)$$

$$\mathrm{Q}_{\mathrm{drain}} = \mathrm{Q}_{\mathrm{drain}_{\mathrm{bot}}} + \mathrm{Q}_{\mathrm{drain}_{\mathrm{top}}} \quad (16)$$

Where
GH_{top} = Groundwater head of top layer (m)
GH_{bot} = Groundwater head of bottom layer (m)
DEU_i = Drainages elevation uppermost (m)
DEL_i = Drainages elevation lowermost (m)
c = drainage conductances (m^2d^{-1})

The groundwater storage (S) was calculated by summing the groundwater storage in the top layer (S_{top}) and bottom layer (S_{bot}). The given equations calculated the groundwater storage for the top layer and bottom layer:

$$\mathrm{S}_{\mathrm{top}} = \max(0, GH_{top} - BULE)\ x\ SC_{top} \quad (17)$$

$$SC_{top} = Sy \quad (18)$$

$$SC_{bot} = \begin{cases} Sy, & \text{if unconfined aquifer} \\ \text{Primary\_Storage\_Coefficient}, & \text{if confined aquifer} \end{cases} \quad (19)$$

$$S_{bot} = \max(0, GH_{bot} - BLLE)\ x\ SC_{bot} \quad (20)$$

Where:
GH_{bot} = Groundwater head of the bottom layer (m)
SC_{bot} = Storage coefficient of the bottom layer (-)
BLLE = Bottom lowermost layer elevation (m)
SC_{top} = Storage coefficient of the top layer (m)
BULE = Bottom uppermost layer elevation (m)
Sy = Specific yield (-)

All of the constant parameters to calculate baseflow and groundwater storage such as river stage elevation, river bed elevation, river bed conductance, drainage elevation (uppermost and lowermost), bottom elevation (uppermost and lowermost), and primary storage coefficient are the output from the "writing tiles parameter" step of GLOBGM simulation. Furthermore, from these eleven baseflow and storage, we conducted a linear regression based on the new non-linear relationship equation which will be explained in the next section.

3.3 Baseflow formula and regression models

Most of the baseflow formula for the non-linear outflow-storage relationship is represented as the Eq.(2) equation. In this study, we develop the equation from Eq.(4). The alpha or recession coefficient is equal to (1/J).

We divided baseflow and groundwater storage with average groundwater storage to make the data less sensitive and improve the model's interpretability. Furthermore, we apply the logarithm to both sides to allow us to do the linear regression analysis. Eventually, we have the following equation for the baseflow-storage relationship:

$$Q = (1/j)\ x\ S_{average}\ x\ (S/S_{average})^{\gamma}$$

$$Q = \alpha\ x\ S_{average}\ x\ (S/S_{average})^{\gamma}$$

$$Q/S_{average} = \alpha\ x\ (S/S_{average})^{\gamma}$$

$$\log(Q/S_{average}) = \log(\alpha) + \gamma\ x\ \log(S/S_{average}) \quad (21)$$

The Eq. (21) allows us to do a linear regression of a non-linear form equation. From the linear regression, we will have the value of the slope or baseflow exponent which is γ, and the intercept which is log (α) for each grid in the global scale. We use the γ or baseflow exponent and α or recession coefficient as the input in the PCR-GLOBWB at 5' resolution.

3.4 PCRGLOBWB 2

3.4.1 General description

PCR-GLOBWB 2.0 is a grid-based global hydrology model with a spatial resolution of 5', which is a recent development model from the first version developed by (Van Beek & Bierkens, 2009). It can simulate moisture storage and water exchange between the soil and the atmosphere. Atmospheric elements simulated by this model include evaporation from bare soil, interception and open water, transpiration, and snow (Sutanudjaja et al., 2018). Runoff from rainfall, snowmelt, and groundwater is routed over the drainage network that encompasses lakes and man-made reservoirs to the ocean. Additionally, PCR-GLOBWB 2.0 also includes water demands from different sectors. PCR-GLOBWB 2 offers the option to be partially or fully coupled with a two-layer groundwater model based on MODFLOW (Sutanudjaja et al., 2011, 2014; de Graaf et al., 2014, 2015,2017).

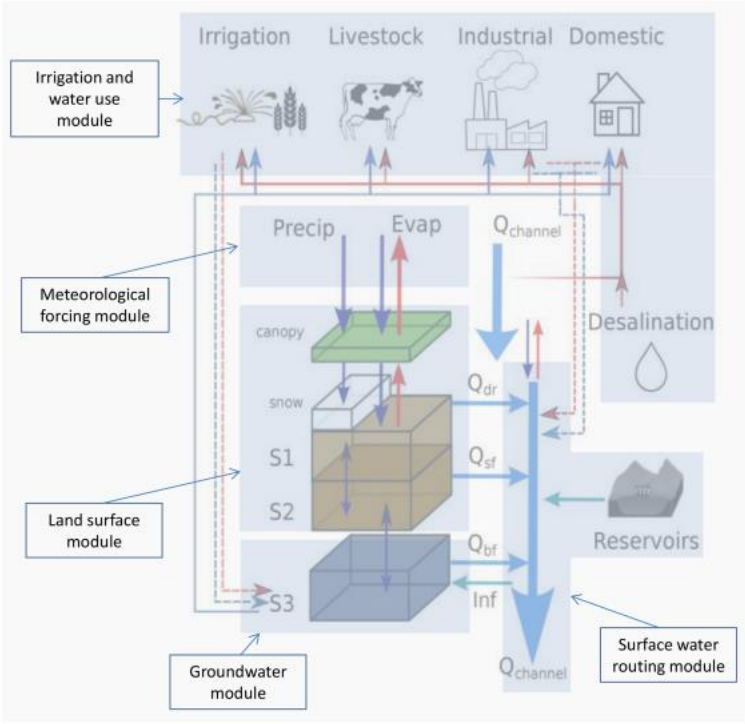

Figure 2 Schematic overview of PCR-GLOBWB 2 modules and structures (Sutanudjaja et al., 2018)

PCRGLOBWB 2 has five main hydrological modules, consisting of a meteorological forcing module, a land surface module, a groundwater module, an irrigation, a surface water routing module, and a water use module (Fig. 2). These module components can be easily modified according to the user's purposes (Sutanudjaja et al., 2018). In this study, the baseflow exponent and recession coefficient parameter in the default groundwater module will be modified for the new moddel. The remaining parameters and forcing input data will be kept unchanged, as specified by Sutanudjaja et al., (2018)

3.4.2. PCR-GLOBWB 2 simulation run

In this research, we simulated two PCR-GLOBWB 2 simulations at the global scale with different drainage settings from 1979 to 2019. The values of the recession coefficient and baseflow exponent were two parameters that varied between these two simulations. In the default model, we used the linear reservoir which has 1 (one) as the single value as the baseflow exponent for the whole grids. In this setup, the recession coefficient is parameterized based on the Kraaijenhov Van de Leur (1958) equation, which was already available in the current PCR-GLOBWB dataset. Meanwhile, in the multiple drainage run, the baseflow exponent and recession coefficient input were obtained from the linear regression of a new baseflow and storage relationship equation from Eq. (21). The baseflow exponent in this new model will vary and we obtained a new recession coefficient value for each grid.

3.4.3 Model evaluation strategy

We employed the Kling-Gupta Efficiency (KGE), a metric (Gupta et al., 2009) that provides three assessment components, such as variability, bias, and correlation, to evaluate the performance of the new model.

The correlation (r) measures the magnitude and the strength of the linear relationship between two variables. The closer the correlation coefficient to 1, the more positive the linear relationship. The second component is bias, which shows the ratio between the mean simulated discharge and observed discharge. The closer the bias to 1, the more equal the mean discharge between these two. The last component is variability, which represents the ratio between the simulated standard deviation and the observed standard deviation.

We used KGE as a metric indicator for our model performance in simulating the discharge. The simulated discharge that has KGE with the range values of $-0.41 < KGE \leq 1$ is considered has a reasonable results (Knoben et al., 2019).In addition to this, we also used the R-squared or coefficient of determination to evaluate the relationship between the simulated and observed discharge to capture the overall pattern and trend of the model, before calculating and breakdown the component of KGE.

3.5 Test area and global

Before implementing on a global scale, the mentioned steps in Fig. 1 were executed in both the Rhine-Meuse basin and Florida. The selection of these areas was strategic. The Rhine-Meuse basin was chosen due to the robust performance of the PCR-GLOBWB model in this region, coupled with the ready availability and accessibility of all necessary data. The basin also includes a variety of catchment features, ranging from the low-lying Netherlands region to the mountainous Alps region in upstream. Conversely, Florida was chosen because it offers a different situation in which PCR-GLOBWB performs rather poorly. This decision facilitates a thorough understanding of the model's strengths and limitations by enabling a comprehensive evaluation of the model's capabilities across various hydrological and geographical contexts.

In the testing area, we ran GLOBGM with the MODFLOW 2005 version. We used this due to the practicability reason. At the time we simulated the tested area, the GLOBGM with MODFLOW 6 was not yet available to use. Furthermore, the new version of GLOBGM using MODFLOW 6 only supports the simulation on the global scale or within one to four of the four region models available. Because of that, using the MODFLOW 2005 version is more reliable in this context. Moreover, the objective of simulating the model in the tested area is to make the iteration process when building the drainage package more flexible. This process also requires less time and simpler computational requirements because we can limit the simulation to the selected area.

We simulated the GLOBGM on a global scale with the MODFLOW 6 after we had succeeded in running the two drainage package setups in the MODFLOW 2005 for the test area and the linear regression from this simulation resulting a reliable result. As a note, there was a difference in the input of the GLOBGM between these two MODFLOW versions. In MODFLOW 2005, the discharge can be simulated directly by the model with the input data of groundwater recharge and total run-off. However, we need to calculate the discharge data ourselves before inputting it into the GLOBGM configuration in the MODFLOW 6 version. The reason for this because in the new GLOBGM version, the area is divided into several tiles, resulting in a disconnected drainage network which makes it is not possible to calculate the discharge by run-off and groundwater recharge within the model itself.

4. Result

4.1 Test area

4.1.1 Baseflow-storage relationship

To analyze the correlation between the baseflow and groundwater storage, we made eleven simulations with the eleven inputs of groundwater recharge and total run-off. The output of baseflow and groundwater storage from this simulation were plotted in the graph, with (baseflow/average groundwater storage) as the y-axis and (groundwater storage/average groundwater storage) as the x-axis. The graph demonstrated the power trendline to capture the non-linearity relationship between the two variables. We plot three different locations for both Rhine-Meuse and Florida.

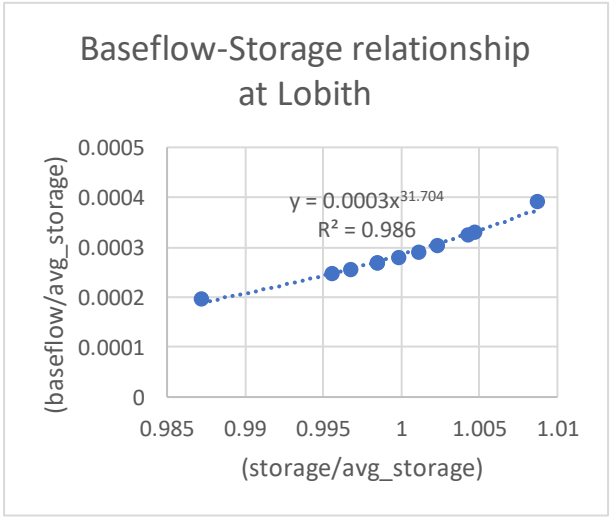

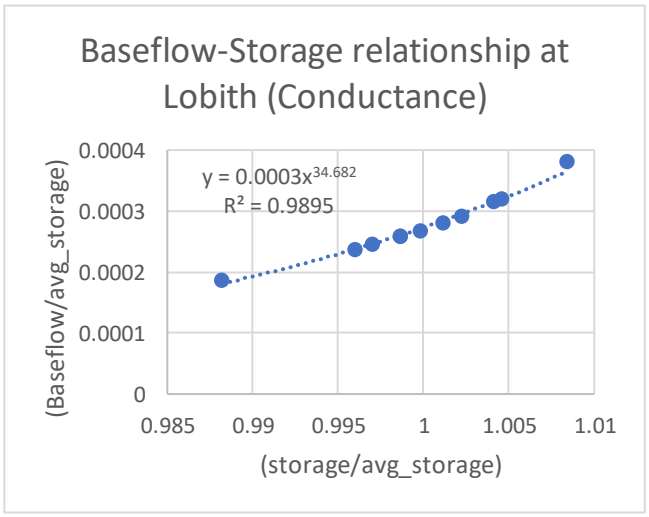

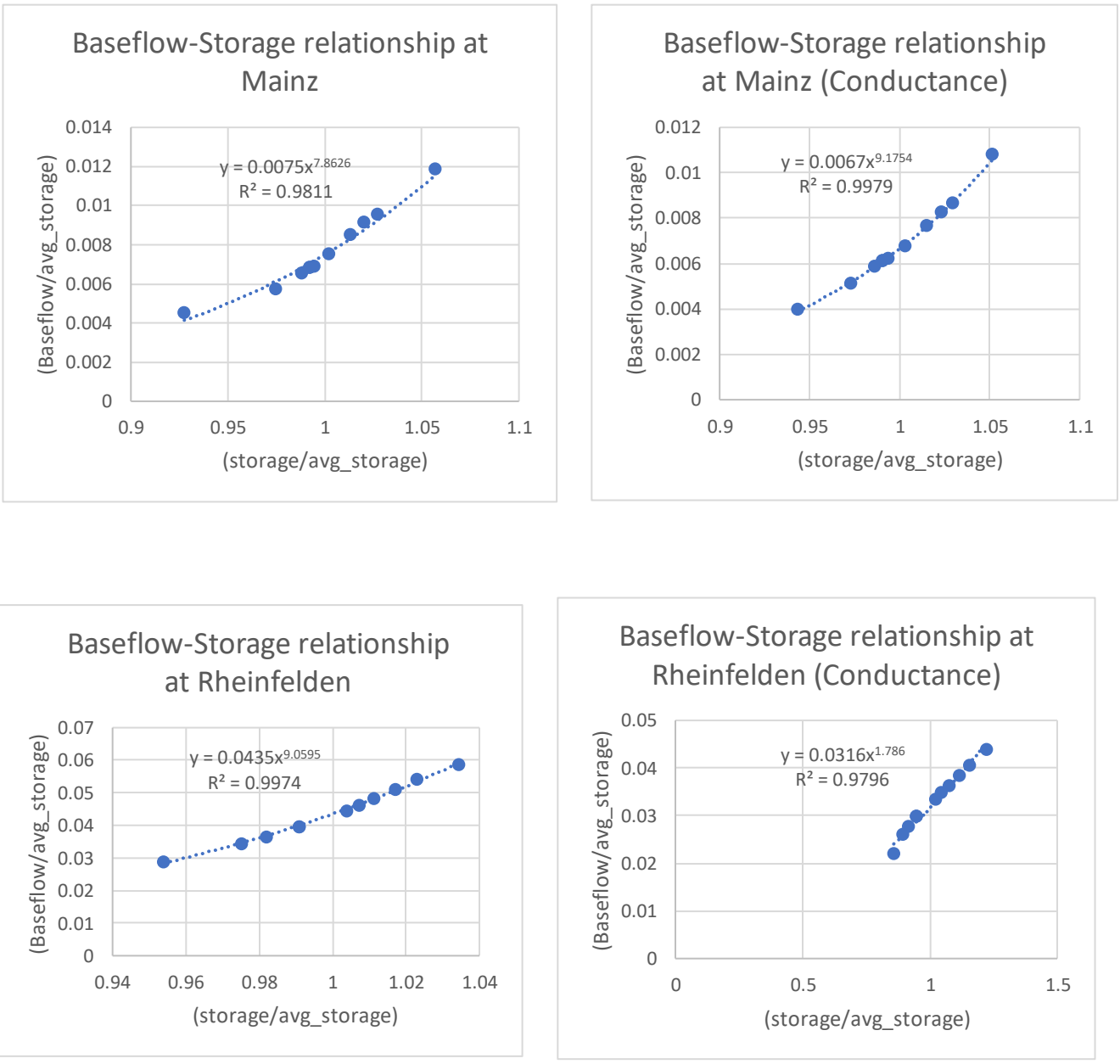

Figure 3 Baseflow and storage relationship in Rhine-Meuse with two different models (Multiple drainages and multiple drainages with various conductances).

Figure 3 above demonstrates the relationship between baseflow and storage for each location under two multiple drainage conditions. The coefficient determination or R-squared value is above 9.85 for every location, which means the correlation between baseflow and storage is well presented by a non-linear relationship, which is a power relationship in this context. In this multiple drainage setup, the power relation fit better in the Rheinfelden area compared to the two other locations in the Rhine-Meuse basin. Furthermore, we also can see that with

the various conductances applied, the relationship between baseflow and storage shows slightly better results for two other areas, unless for Rheinfelden.

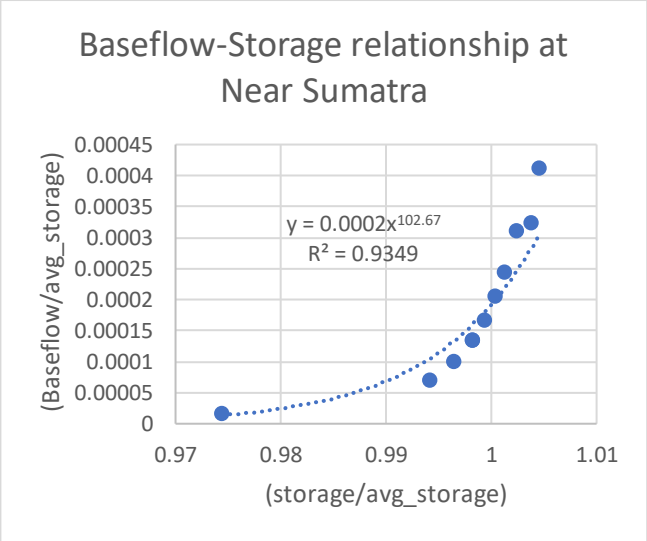

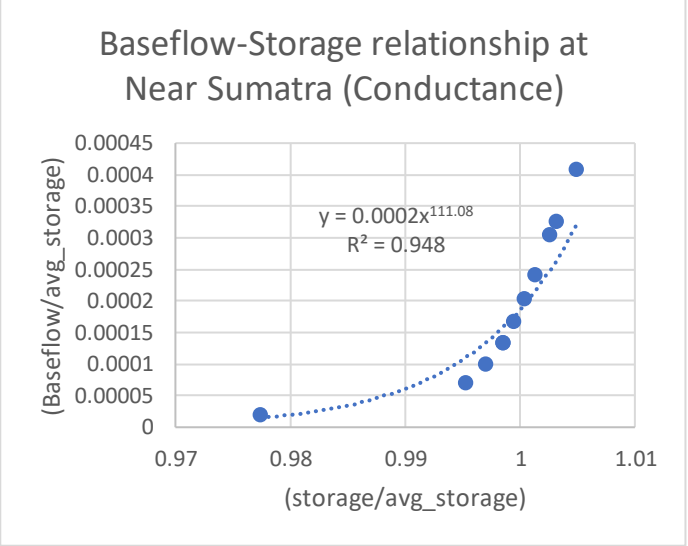

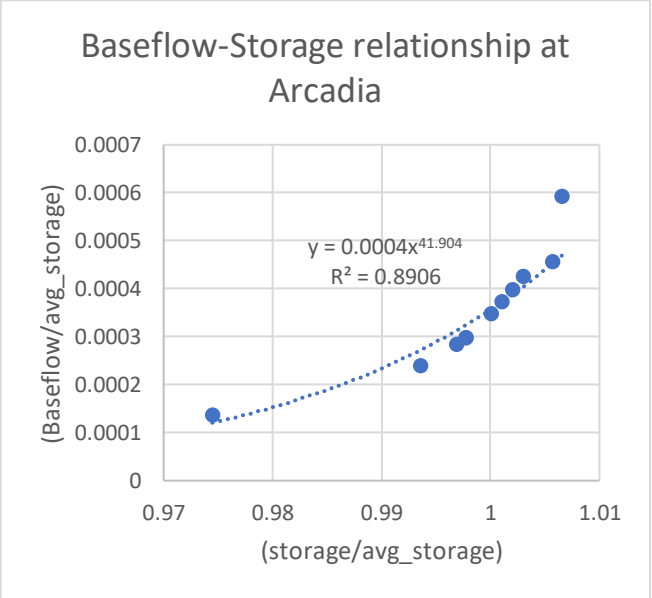

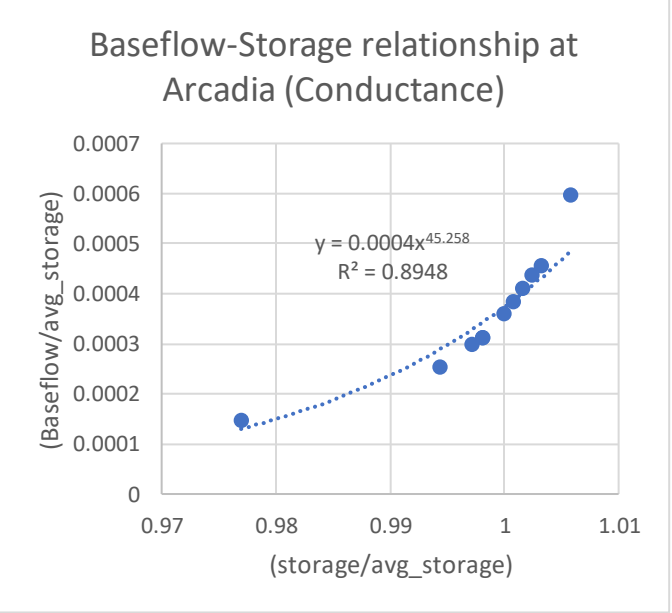

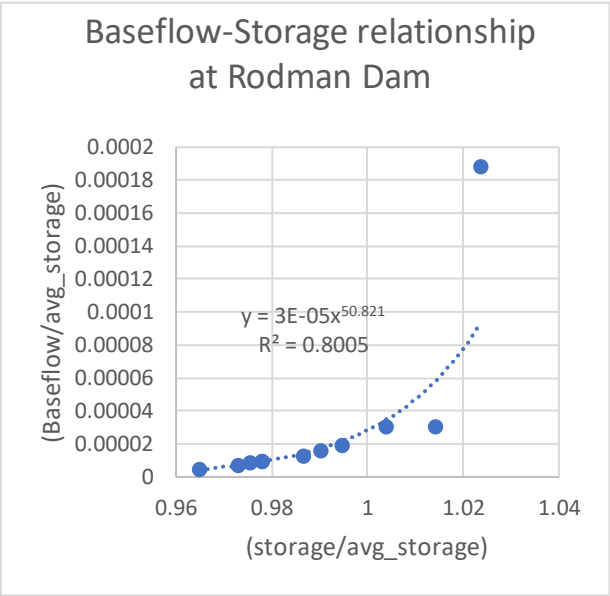

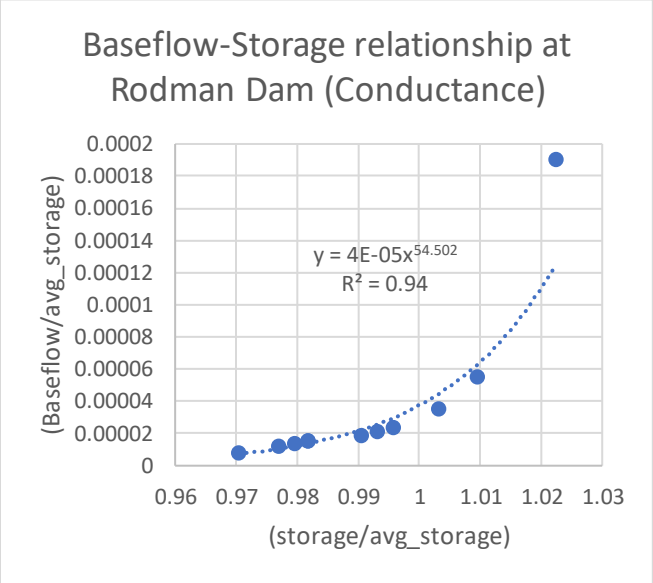

Figure 4 Baseflow and storage relationship in Florida with two different models (Multiple drainages and multiple drainages with various conductances).

The non-linear relationship between baseflow and storage is also shown in Florida. Although the determination coefficient is lower than Rhine-Meuse, it still has a high value. The power relationship fits better in the multiple drainages with various conductance packages for every location. The most significant difference of R-squared occurs at Roadman Dam, where it increases from 0.8005 under the multiple drainages concept to 0.94 when the various conductances are applied. Based on these six locations, a model shows a better fit when we incorporate the various conductances concept into the model.

4.1.2 R-squared, intercept, and slope

This chapter will present the spatial distribution of its R-squared, slope, and intercept. From Fig. 5 below, the R-squared for Rhine-Meuse and Florida predominantly have a high R-squared. In the Rhine-Meuse, the area with a low R-squared is mountainous, especially in the Alps. A similar correlation also happens in Germany (pink color). The map below shows that the high R-squared is also distributed better in Rhine-Meuse compared to Florida.

The red color, which shows the high R-squared is not too dominant, and is mostly mixed up with green to yellow color in Florida. Additionally, most of the low R-squared is in the northern part of the region.

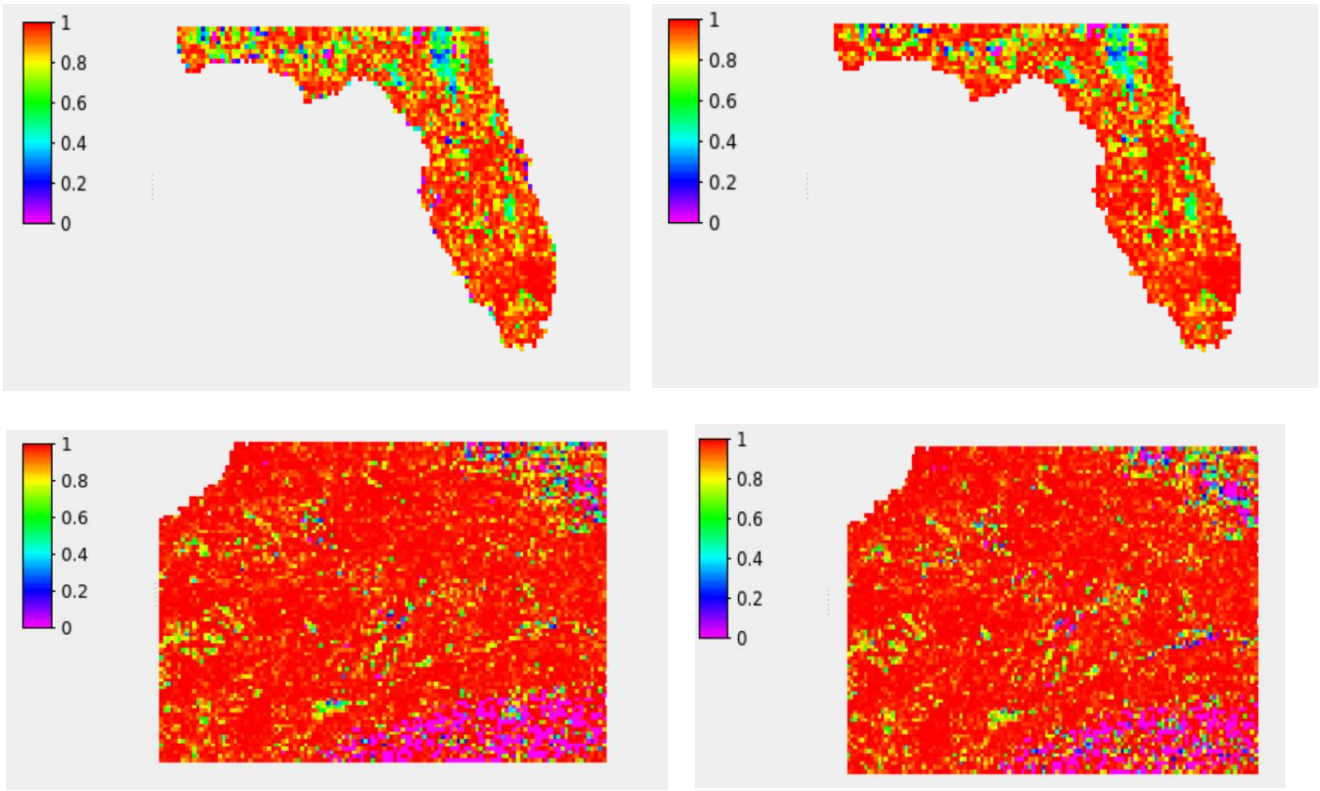

Figure 5 R-squared spatial distribution map in Florida with multiple drainages (left-top), various conductances (right-top), Rhine-Meuse with multiple drainages (left-bottom), and various conductances (right-bottom)

The maps in Fig. 6 show the intercept value distribution from the baseflow-storage linear regression. The intercept value in this map is in the logarithmic form (log α), so it should be calculated by performing ten powers of the intercept value to obtain the recession coefficient (α). The interception shows the base level of baseflow relative to the average of groundwater storage. Hence, the higher the intercept, the higher the baseflow in that area.

It can be seen that some area has a negative intercept value, indicating this area has a very low baseflow relative to average storage. However, the intercept value does not solely determine the amount of baseflow. The slope is also an important indicator to analyze the contribution of baseflow from the groundwater storage. The slope or baseflow exponent determines the magnitude and demonstrates the sensitivity of baseflow to the change in groundwater storage. The higher the slope, the more sensitive the baseflow shift due to the change of the storage.

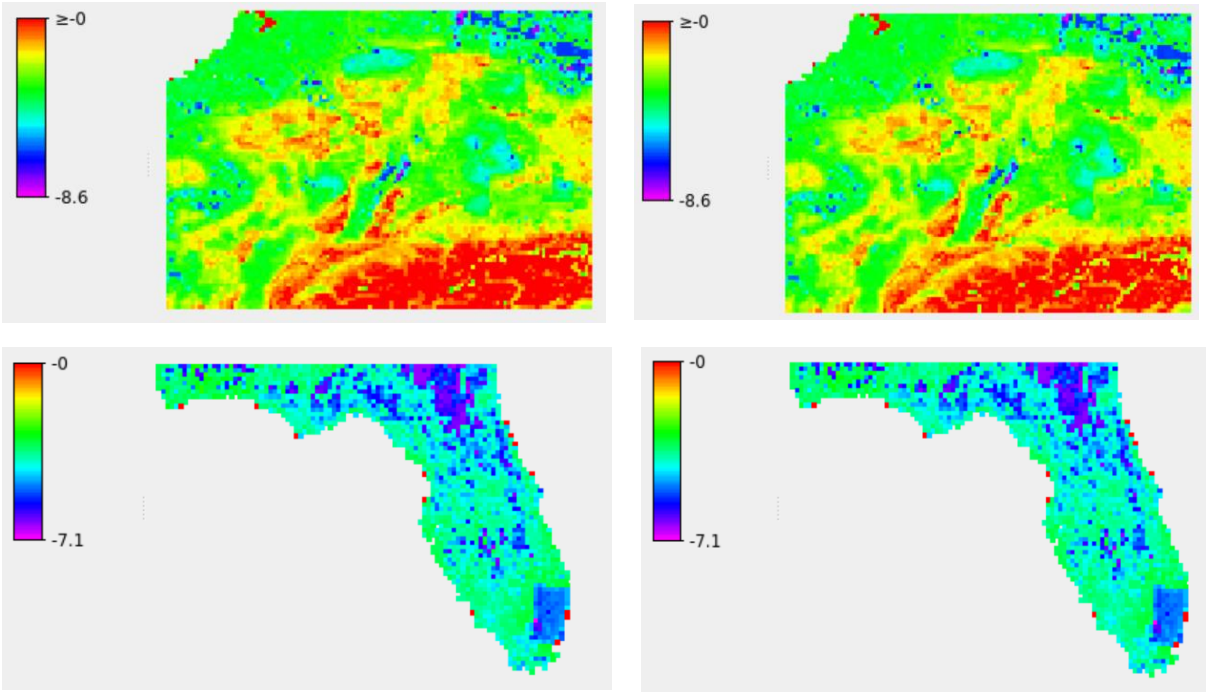

Figure 6 Intercept value spatial distribution map in Florida with multiple drainages (right-bottom), various conductances (left-bottom), Rhine-Meuse with multiple drainages (left-top) and various conductances (right-top)

We can take the example of the red Alps area, which has a low slope (pink color) and high intercept (red color). This area has a high baseflow, indicating the water level does not change significantly due to the change of the groundwater storage. The reason for this because the sources of baseflow in this area do not solely come from the groundwater storage but also from the unconfined aquifer, direct run-off, groundwater seepage, or snowmelt.

On the contrary, most areas in the Rhine-Meuse Basin and Florida have high slopes (red color) and low intercepts (pink color). Under the average storage condition, the baseflow from this area is very low even has no baseflow. Particularly for the area with negative intercept, the groundwater recharge in this area will refill the storage first before contributing to the baseflow. Therefore, this area is very sensitive to the change in groundwater storage, which means the baseflow mainly comes from the storage and the small changes within it will significantly influence the amount of baseflow.

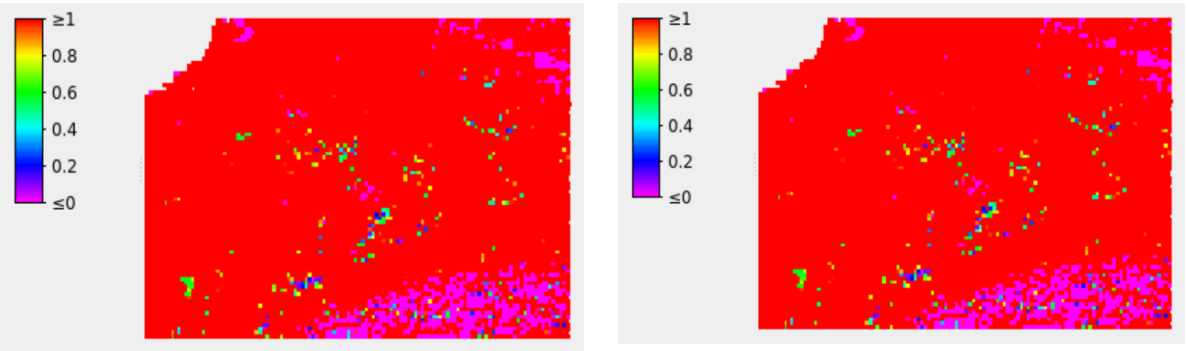

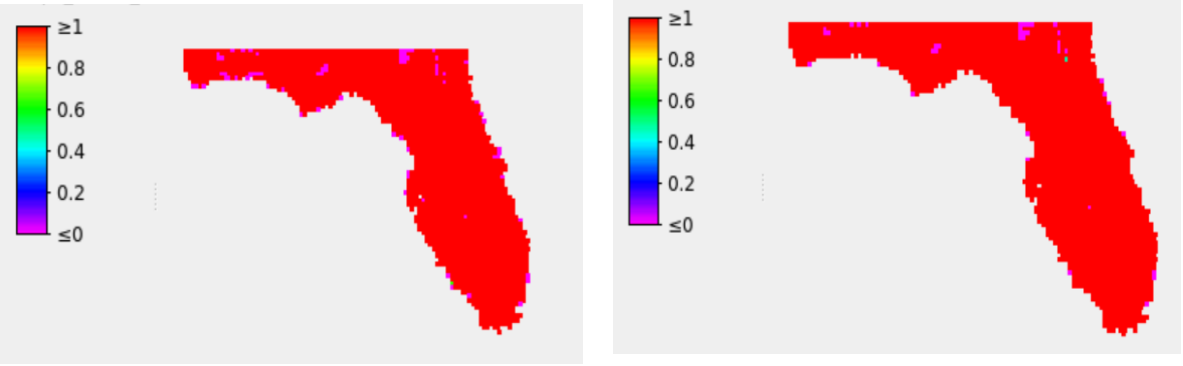

Figure 7 Spatial distribution map of the slope value in Florida with multiple drainages (right-bottom), various conductances (left-bottom), Rhine-Meuse with multiple drainages (left-top) and various conductances (right-top)

4.1.3 Discharge

For result analysis, we used the observation data based on GRDC from 1979 until the latest year available. We used coefficient determination or R-squared to see how the model captures the variability or data's pattern, especially the precision when the time of discharges increases or decreases compared to the observation data. For the more comprehensive analysis, we determined the Kling Gupte Efficiency or KGE which demonstrates a more holistic measure for model performances.

In general, the simulated discharge for the Rhine-Meuse Basin demonstrates a better R-squared performance than the current default model. This indicates that the model more accurately captures the pattern and timing of flow increases or decreases. However, the KGE for the two new setup models shows a lower performance compared to the existing ones. The graph below illustrates that the discharge in two new simulation models often exhibits a very high bias and variability, resulting in higher peaks than those observed in the actual data.

The multiple drainages model performs better in terms of R-squared at the Lobith and Mainz, with values of 0.9146 and 0.85743 respectively, while the multiple drainages with various conductances perform better at Rheinfelden with a value of 0.65306. Furthermore, the multiple drainage model has a similar KGE, with only very small differences compared to the multiple drainages with various conductances across all three locations in the Rhine-Meuse Basin.

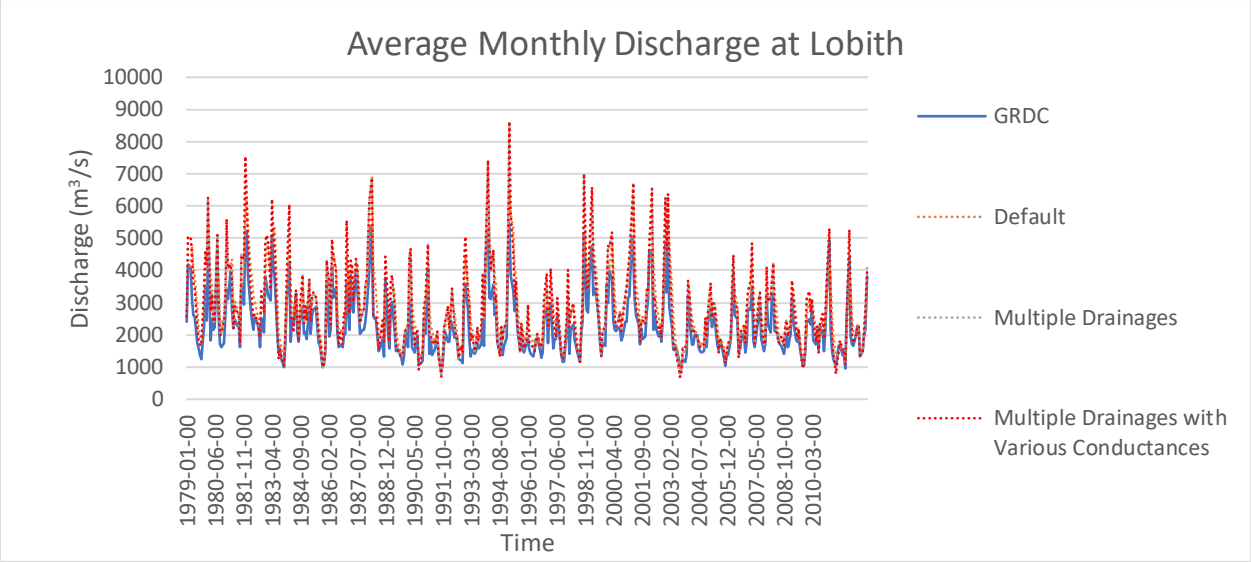
Average Monthly Discharge at Lobith
Discharge (m³/s)
10000
9000
8000
7000
6000
5000
4000
3000
2000
1000
0
1979-01-00
1980-06-00
1981-11-00
1983-04-00
1984-09-00
1986-02-00
1987-07-00
1988-12-00
1990-05-00
1991-10-00
1993-03-00
1994-08-00
1996-01-00
1997-06-00
1998-11-00
2000-04-00
2001-09-00
2003-02-00
2004-07-00
2005-12-00
2007-05-00
2008-10-00
2010-03-00
Time
GRDC
Default
Multiple Drainages
Multiple Drainages with Various Conductances

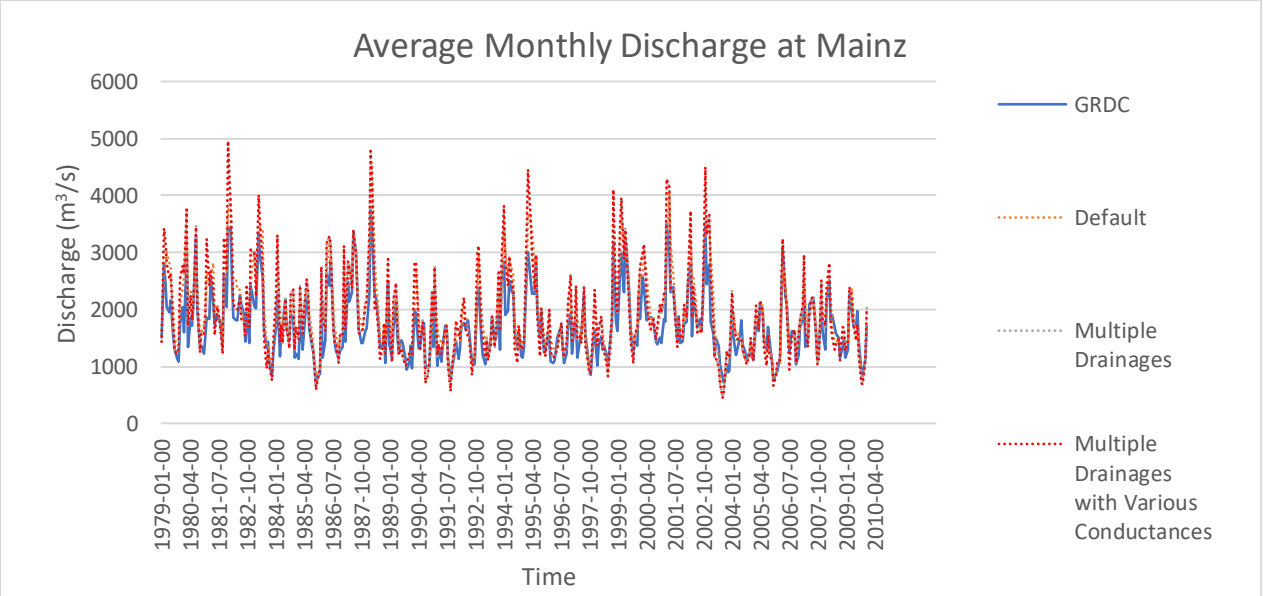
Average Monthly Discharge at Mainz
Discharge (m³/s)
6000
5000
4000
3000
2000
1000
0
1979-01-00
1980-04-00
1981-07-00
1982-10-00
1984-01-00
1985-04-00
1986-07-00
1987-10-00
1989-01-00
1990-04-00
1991-07-00
1992-10-00
1994-01-00
1995-04-00
1996-07-00
1997-10-00
1999-01-00
2000-04-00
2001-07-00
2002-10-00
2004-01-00
2005-04-00
2006-07-00
2007-10-00
2009-01-00
2010-04-00
Time
GRDC
Default
Multiple Drainages
Multiple Drainages with Various Conductances

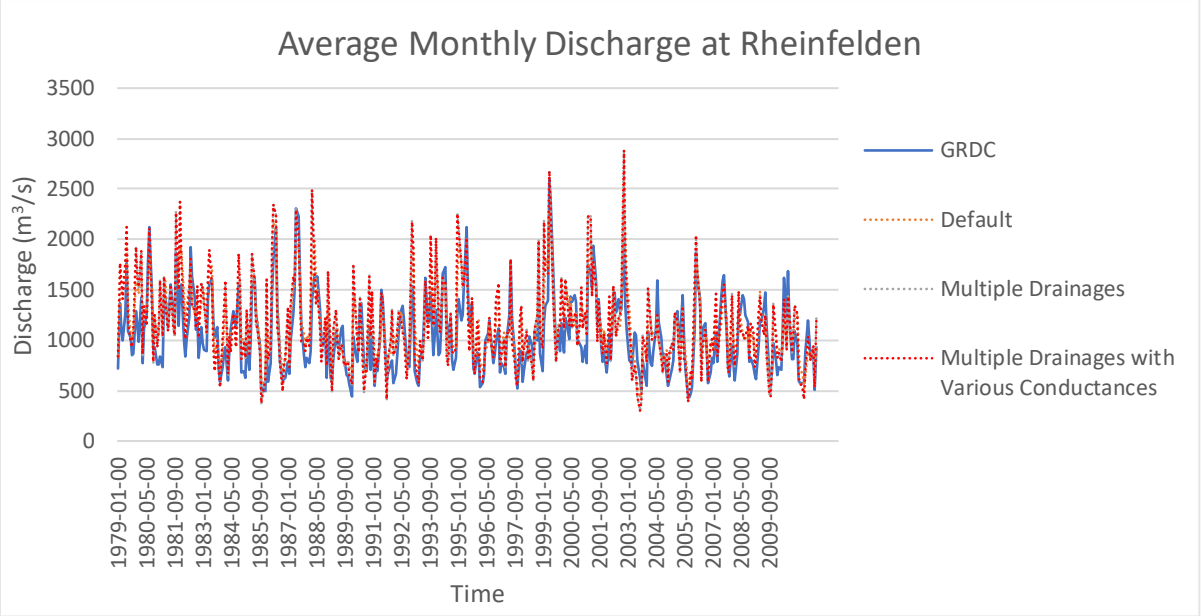
Average Monthly Discharge at Rheinfelden
Discharge (m³/s)
3500
3000
2500
2000
1500
1000
500
0
1979-01-00
1980-05-00
1981-09-00
1983-01-00
1984-05-00
1985-09-00
1987-01-00
1988-05-00
1989-09-00
1991-01-00
1992-05-00
1993-09-00
1995-01-00
1996-05-00
1997-09-00
1999-01-00
2000-05-00
2001-09-00
2003-01-00
2004-05-00
2005-09-00
2007-01-00
2008-05-00
2009-09-00
Time
GRDC
Default
Multiple Drainages
Multiple Drainages with Various Conductances

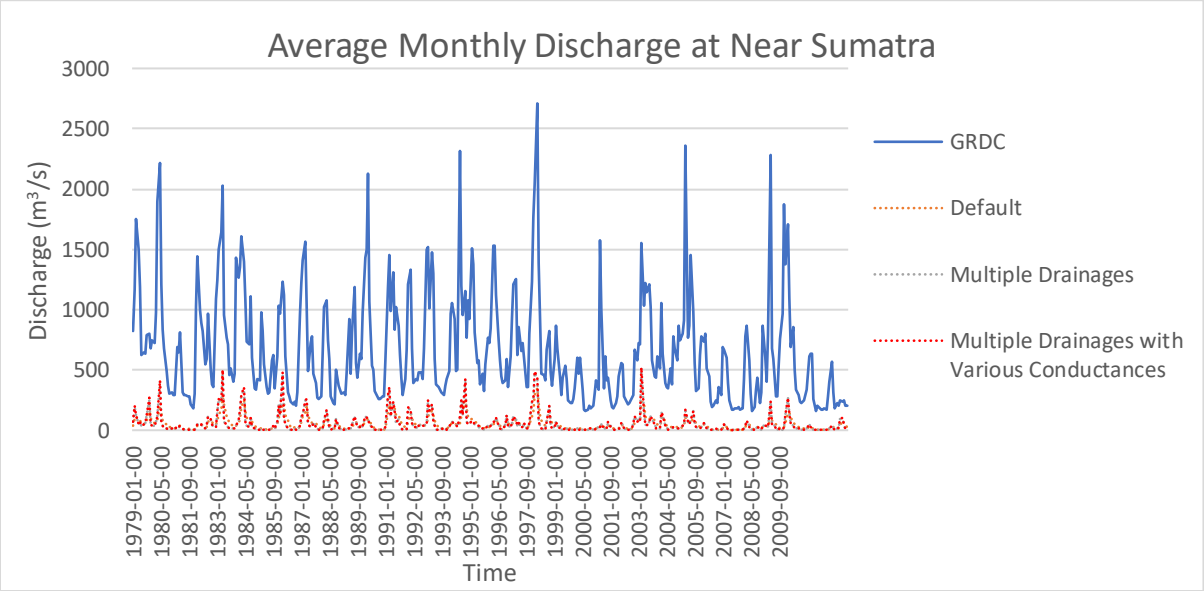
Average Monthly Discharge at Near Sumatra
Discharge (m³/s)
3000
2500
2000
1500
1000
500
0
1979-01-00
1980-05-00
1981-09-00
1983-01-00
1984-05-00
1985-09-00
1987-01-00
1988-05-00
1989-09-00
1991-01-00
1992-05-00
1993-09-00
1995-01-00
1996-05-00
1997-09-00
1999-01-00
2000-05-00
2001-09-00
2003-01-00
2004-05-00
2005-09-00
2007-01-00
2008-05-00
2009-09-00
Time
GRDC
Default
Multiple Drainages
Multiple Drainages with Various Conductances

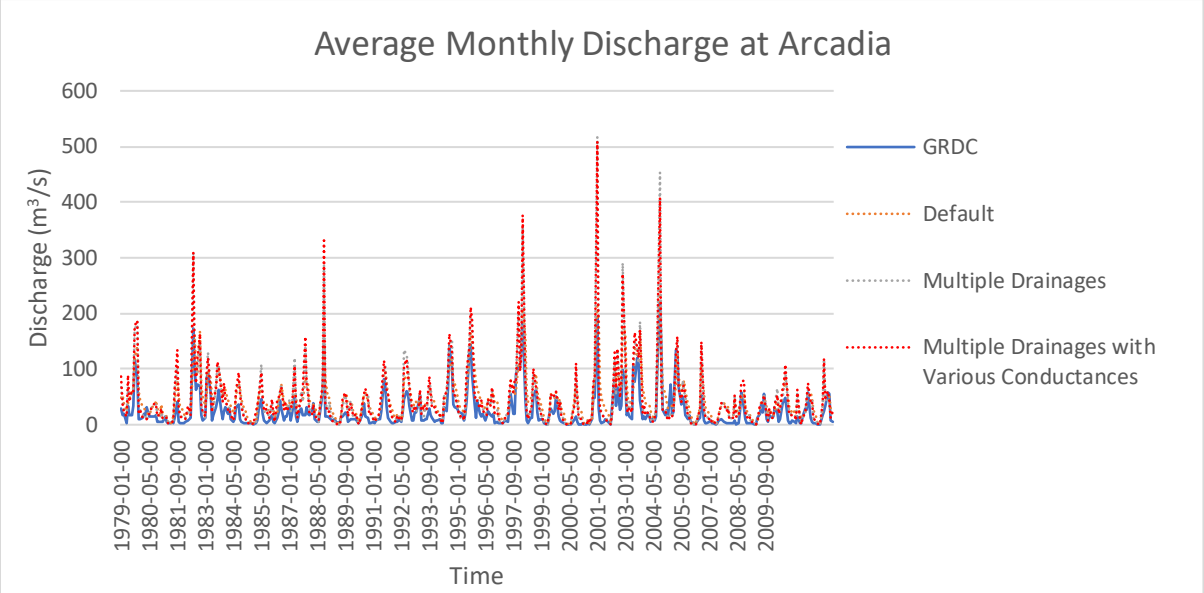

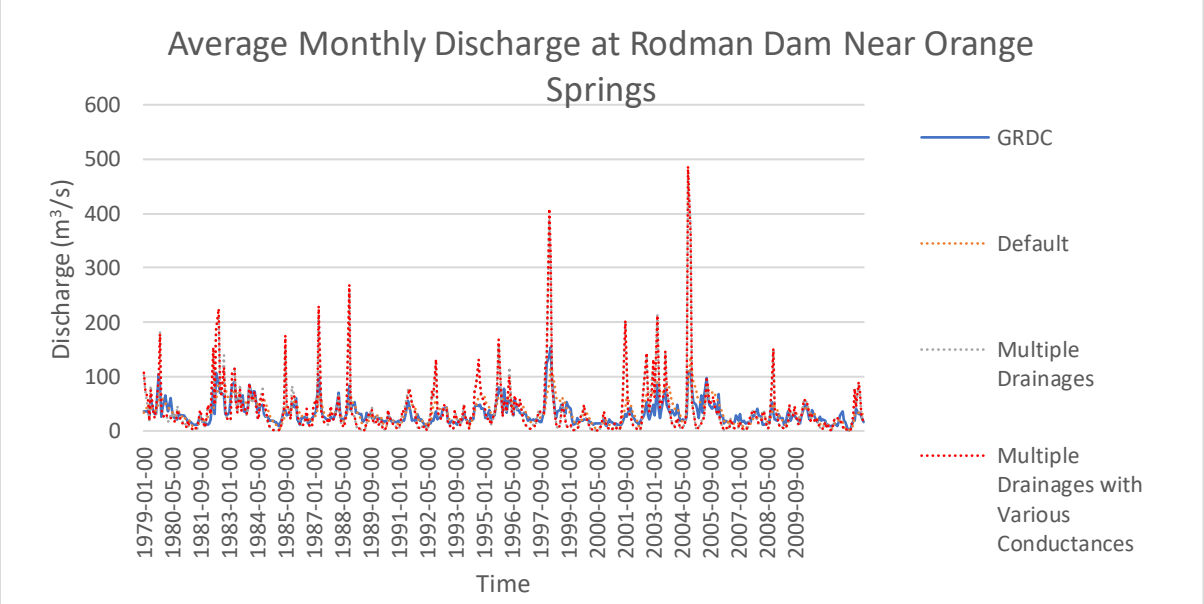

Figure 8 Hydrograph for 3 locations in Rhine-Meuse and Florida. The blue line shows the GRDC observation discharge, the orange dot line shows the simulated discharge with the default model, the grey dot line shows the simulated discharge with multiple drainages model, and the red dot line shows the simulated discharge with multiple drainages and various conductances model

In general, all of the three model setup in this study simulate better results in the Rhine-Meuse rather than Florida. The highest R-squared from the three locations in Florida occurs at the Arcadia, with a value of 0.743063 for the multiple drainage model and 0.756638 for multiple drainage with various conductances model. The multiple drainage model with various conductances performs better at the Arcadia and Roadman Dam, whereas the multiple drainage model has a better R-squared at the Near Sumatra.

Specifically at the Near Sumatra, PCR-GLOBWB performs a very poorly performance in all three models. We can see from the Fig. 8 above, that the model does not fit the observation data and exhibits a significant discrepancy.

4.2 Global implementation

4.2.1 R-squared

We used the R-squared indicator to see the correlation between baseflow and groundwater storage. If the R-square value is closer to 1, it suggests a strong correlation, meaning the model can effectively explain the variance in baseflow based on storage.

A high R-square value predominantly occurs in the high or stable precipitation rate. Fig.9 demonstrates that the high R-squared are represented with green to red color as the highest. It includes the Northern and Western European countries like Germany, Switzerland, Norway, France, Sweden and Finland. Moreover, similar values are distributed in the Eastern part of the United States and Canada. The mentioned areas mostly have a robust data monitoring system.

However, it does not mean that the less developed regions with less monitoring data available have a low R-squared, the model also shows a good fit in some countries like Peru, Chile, some parts of Brazil, and the coastal areas of South America. In the other continent, the model also performs well such as in the West and Central African countries such as Ghana, Côte d'Ivoire, Liberia, Nigeria, Sierra Leone, and Congo. Additionally, the model also fits well in densely populated areas like China (Eastern and Southern), and South-East Asian regions (excluding the island countries).

The opposite pattern is exhibited in arid regions such as the eastern part of Saudi Arabia, Kuwait, UAE, Iraq, Syria, central Australia, and the southern part of the Sahara. Low R-squared values are also observed in regions like Central Asia and Northern Canada.

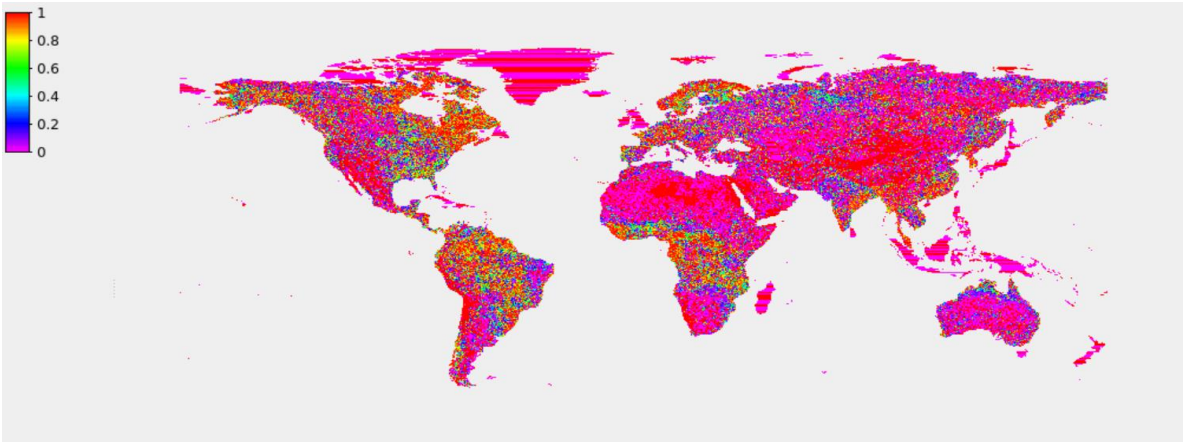

Figure 9 Spatial distribution of the R-squared map for global scale

4.2.2 Slope and intercept

Because some areas have a low R-squared, we created composite values for both slope and recession coefficient (10 power of intercept). The purpose of this is to reduce the misvalued in the area that has a very low R-squared. The composited slope and recession coefficient were calculated by the following equations:

$$\text{Composite slope} = (R\_square \times new\_slope) + ((1-R\_square) \times 1) \quad (22)$$

$$\text{Composite recession coefficient} = (R\_square \times new\_recession\_coefficient) + ((1-R\_square) \times default\_recession\_coefficient) \quad (23)$$

The intercept indicates the baseflow level of an area relative to the average groundwater storage. The higher the intercept, the more the baseflow level in the area even if without significant changes in the groundwater storage. Low intercept values, represented by blue to pink colors, are found in arid climate regions, resulting in low baseflow levels, including the area such as the Middle East, the desert regions of North Africa, and Central Australia. Furthermore, the regions with low precipitation, such as Northern China and Central Asia, also exhibit low intercept values. In Eastern Europe, the areas with less precipitation and hydrological connectivity, particularly areas near Russia, show low intercept values. Similarly, Northern Canada and the Northern part of Russia have low intercept values due to the presence of permafrost and harsh climate conditions.

Conversely, high intercepts are represented by green to red colors. High intercept values are typically found in areas with high precipitation. These include dense forests and tropical regions such as the Amazon basin, Congo basin, and Southeast Asian countries. Mid to high intercept values are also observed in moderate climates with stable precipitation, such as Western Europe and the Eastern part of the United States.

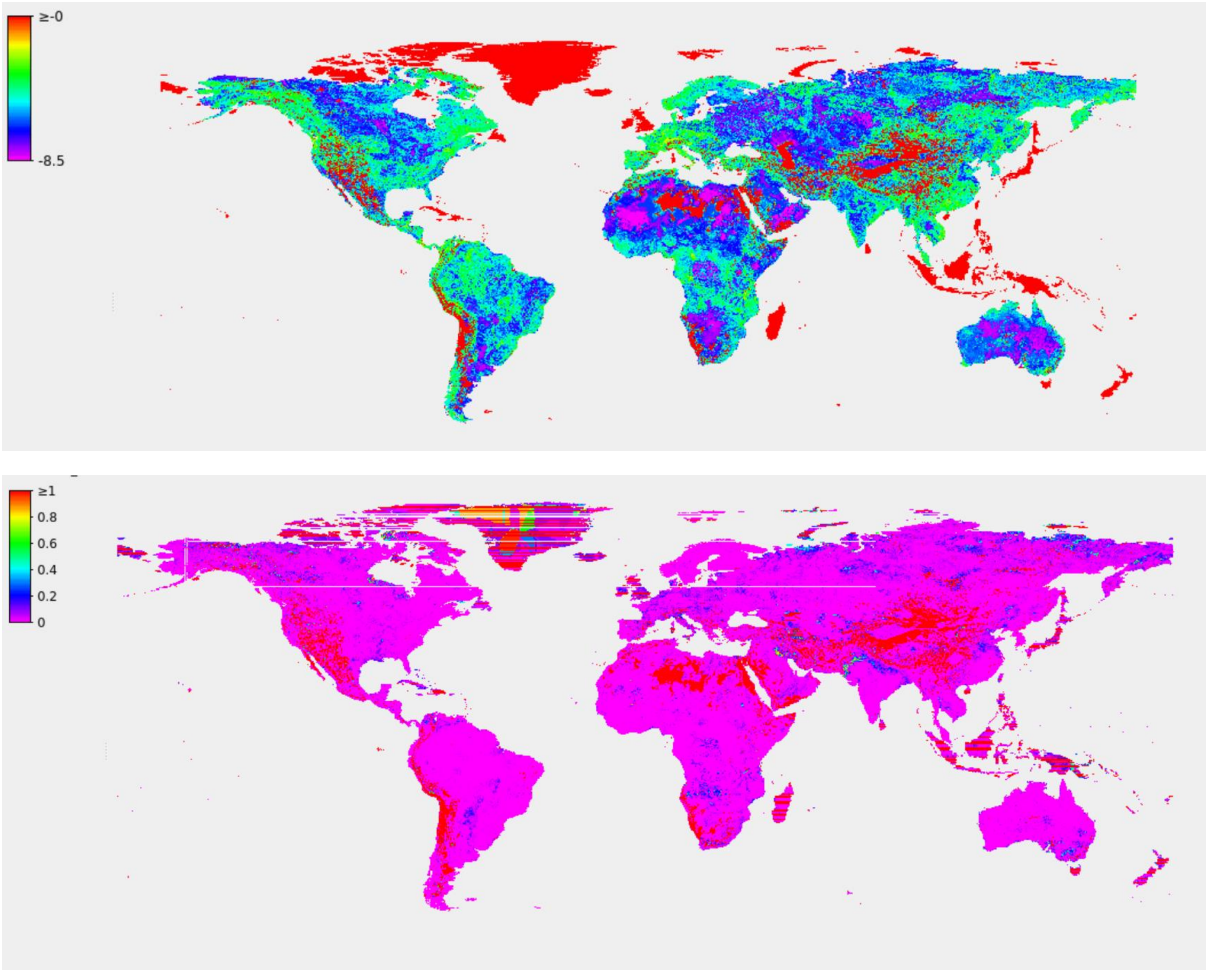

Figure 10 Illustration of the intercept values that indicate the base level of baseflow relative to the average of groundwater storage (top) and recession coefficient values (bottom)

The slope distribution has a similar pattern to the intercept. Low slope values are found in arid climate regions such as Central Australia, the Sahara desert, the Western part of the United States, and the Middle East. In addition to this, the areas with low precipitation, including Southern Africa, Central Asia, and the Indus Basin in Pakistan, also exhibit low slope values. Baseflow in this region has an inverse correlation with the change in groundwater storage. It means the baseflow decreases when the storage increases. This occurs due to low precipitation, high evaporation rates, and significant vegetation water use.

Regions with positive slopes are depicted in colors ranging from blue to red, with red indicating the highest slope values. The higher the slope in the area, the more sensitive the baseflow to the change of groundwater storage. Areas with high slope values include tropical regions with high precipitation rates, such as the Amazon Basin, Congo Basin, Yangtze River Basin, Pearl River Basin, Ganga-Brahmaputra Basin, and Southeast Asia. In the European continent, countries like Germany, France, Northern Italy, Finland, Sweden, Norway, Eastern Russia, and Switzerland have high positive slope values due to moderate rainfall and snow precipitation. Additionally, the Eastern United States and Eastern Canada

also experienced conditions similar to those in Western Europe, resulting in high positive slope values.

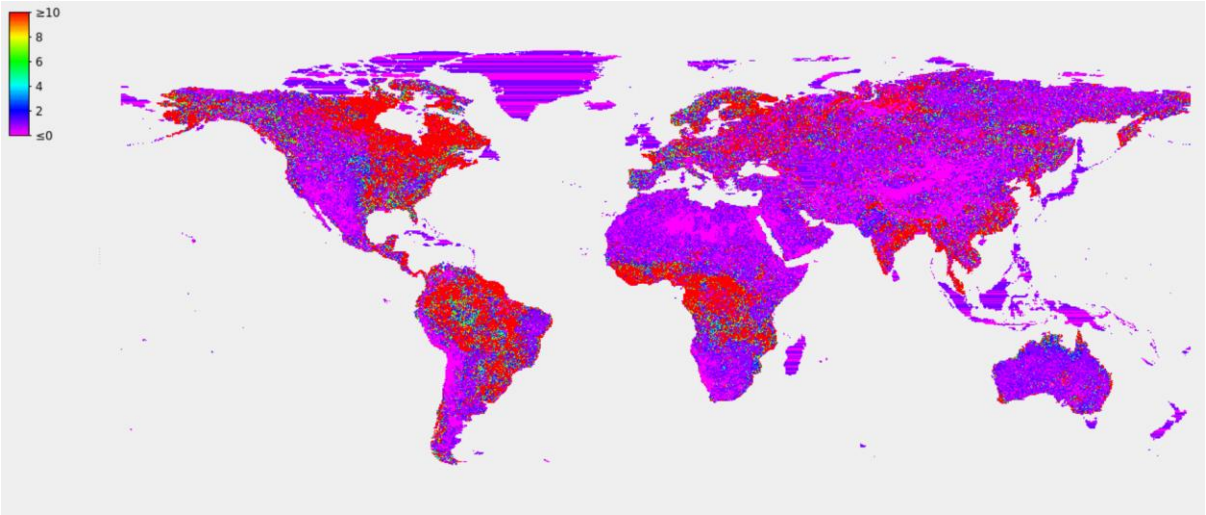

Figure 11 Illustration of the slope values that indicate the sensitivity of baseflow to the change of groundwater storage. Positive values, represented by colors ranging from blue to red, signify a positive slope, where an increase in storage leads to an increase in baseflow. In contrast, negative values, shown in pink, indicate a negative slope.

4.2.3 KGE and R-squared of global discharge

Figure 12 illustrates the comparison between the default model, represented by the black line, and the new multiple drainages model, represented by the red line. The black line consistently shows better performance overall. Specifically, the default model demonstrates that 45% of the KGE values are less than -0.4, whereas the new model shows that 50% of the KGE values fall below this threshold.

However, both models display a similar pattern when considering higher KGE values. The cumulative distribution indicates that 20% of the stations have a KGE value greater than 0.5 for both models. While the default model maintains a superior overall KGE value, it is important to note that the new model shows improvements in specific stations.

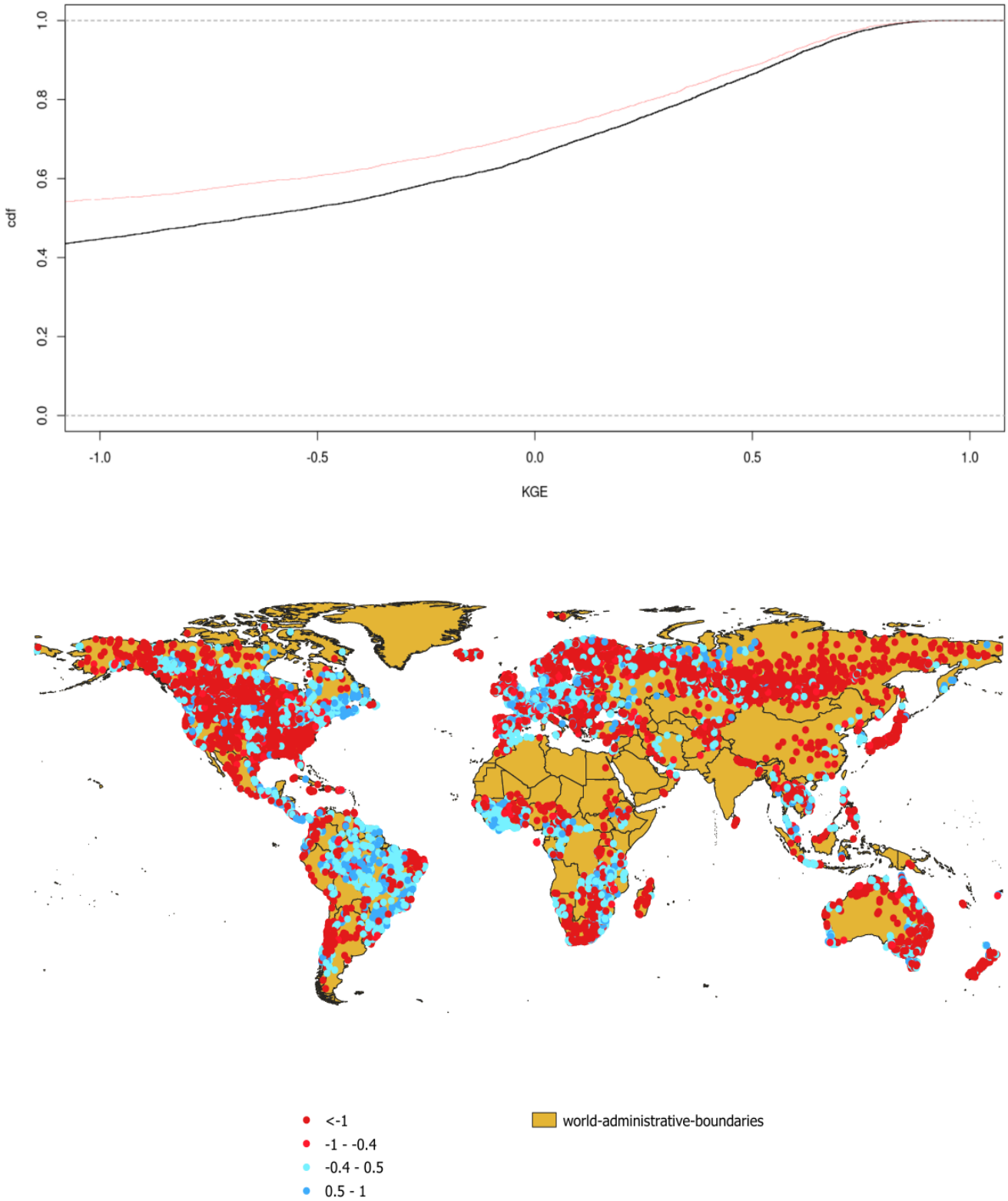

Figure 12 Cumulative Distribution Function (CDF) of KGE for the multiple drainage model which is represented by the line and default model represented by the black line (top) and spatial KGE distribution for the new model (below)

The spatial distribution of the KGE improvement can be seen in Fig. 13. The map shows the subtraction between the KGE in our new model in this study and the KGE in the default model. The blue dots on the map indicate areas where the KGE has increased, signifying improved model performance, whereas the red dots illustrate the opposite.

The map shows that the KGE improvements occurred in tropical regions such as South America, Central Africa, and Southeast Asia, as well as in temperate climates like Western-Northern Europe and the eastern parts of the United States and Canada. On the contrary, the multiple drainage model shows worse performance in semi-arid regions, including the Middle East, Southern Africa, and Northern Africa, as well as in tropical non-forest areas in South America, and continental climate zones such as Northern Russia and Northern Canada.

To evaluate the model's ability to capture data variance, we also plotted the determination correlation (R^2) between the simulated discharge and the GRDC observed discharge, comparing the two models. Figure x illustrates that the new model demonstrates a greater improvement in R-squared compared to KGE. This is evident from the distribution of more blue dots compared to the red dots.

The increase of R-square is not always accompanied by the increase of KGE. For instance, at the Lobith Station, Rhine River in the Netherlands. To investigate this, we created Cumulative Distribution Function (CDF) curves for each component of the KGE: variability, bias, and correlation. These CDF curves help us understand the specific factors contributing to the differences in model performance.

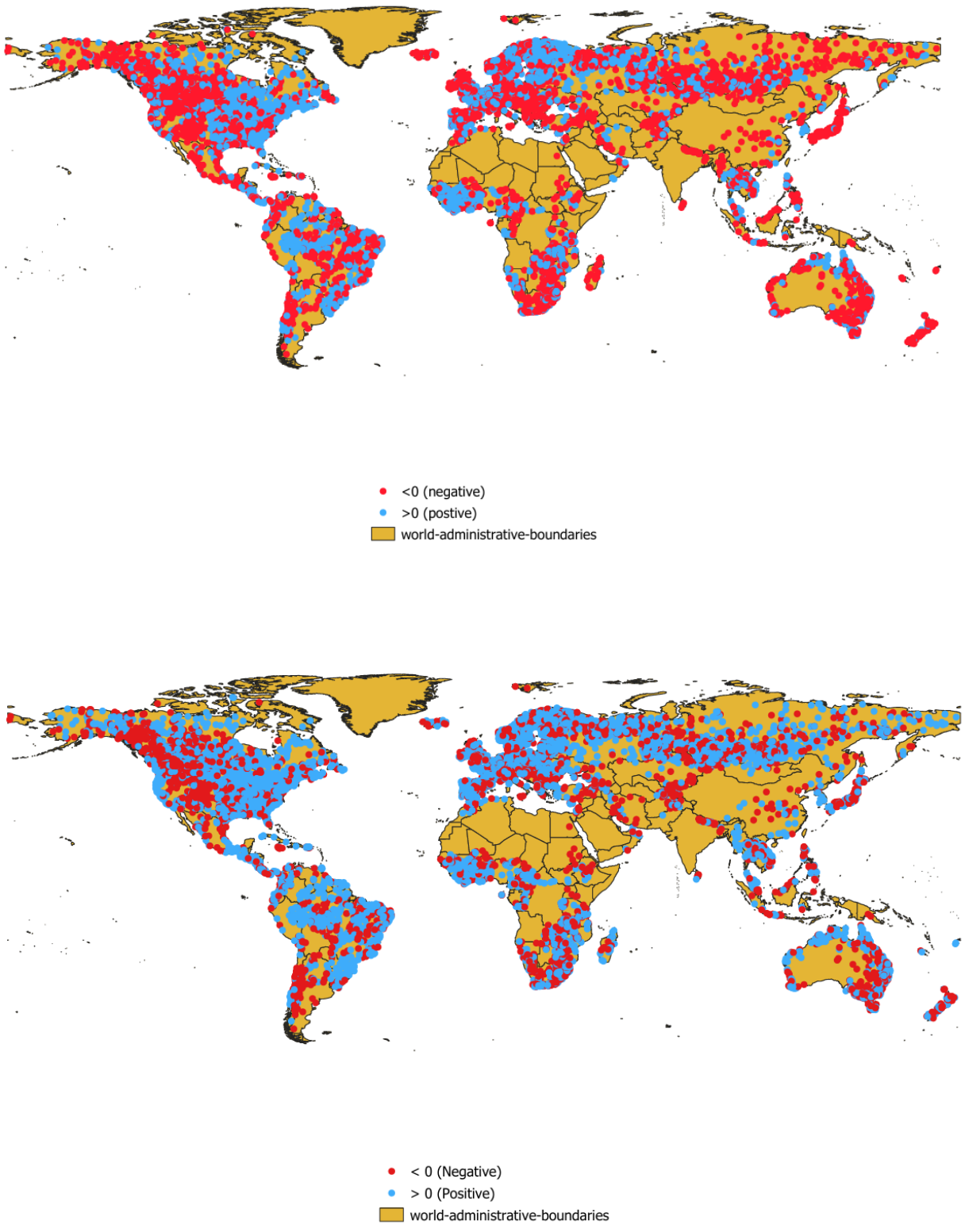

Figure 13 The spatial distribution of KGE difference (top) and R-squared difference (bottom) between the new model and default model. A positive or blue color means there is an improvement in the new model

The blue line depicts the default model, while the green line represents the new model. The first graph in the Fig. 4 illustrates variability. The new model consistently shows low variability, which might result in it overlooking some extreme events. Conversely, the default model demonstrates a larger portion of the area with variability values closer to 1, indicating better alignment with the observed data.

Next, we examine the bias component. The default model has a larger portion of bias that is closer to 1 and a wider range of bias compared to the new model. The new model shows a very low bias, with around 80% of the data having a bias lower than 0.1, whereas the default model has about 60% of the data within this range. This indicates that the means simulated discharge from the new model is significantly lower than the observed data. However, the default model simulated more overestimated discharge compared to the new model. It is demonstrated by the CDF curve which shows that the default model has approximately 15% of data with a bias greater than 10, while the new model has only 5% of the data with such a high bias.

The last component of KGE is correlation. Overall, there is an improvement in correlation with the new model. As shown in Fig. 14, the multiple drainage model has a greater number of locations with a correlation value greater than 0.4. This means a new model can better capture the pattern and temporal dynamic of the discharge.

.

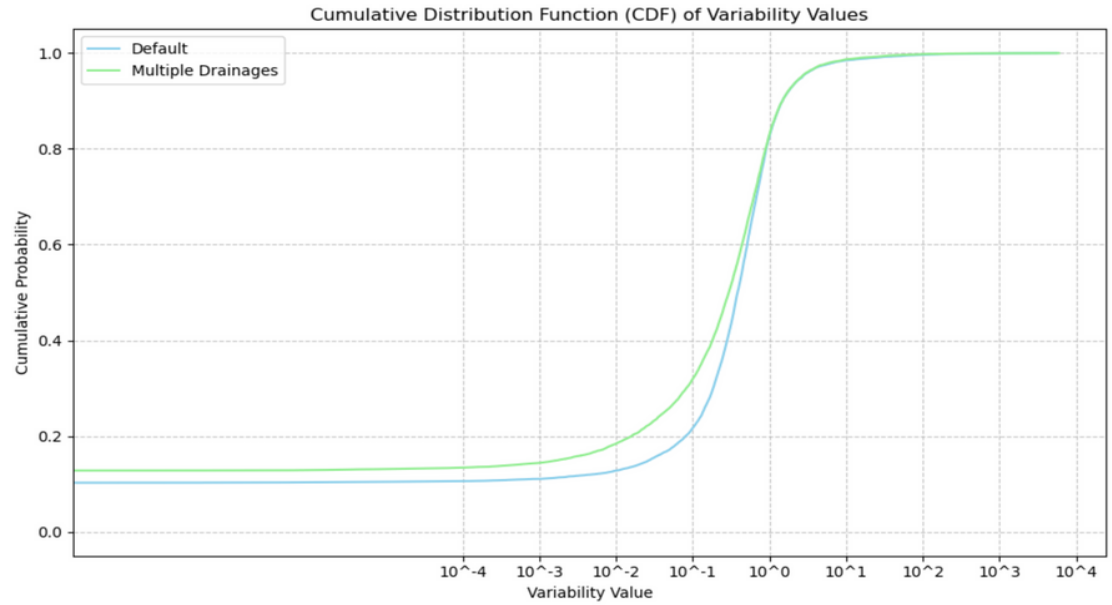
Cumulative Distribution Function (CDF) of Variability Values
Default
Multiple Drainages
Cumulative Probability
1.0
0.8
0.6
0.4
0.2
0.0
10^-4
10^-3
10^-2
10^-1
10^0
10^1
10^2
10^3
10^4
Variability Value

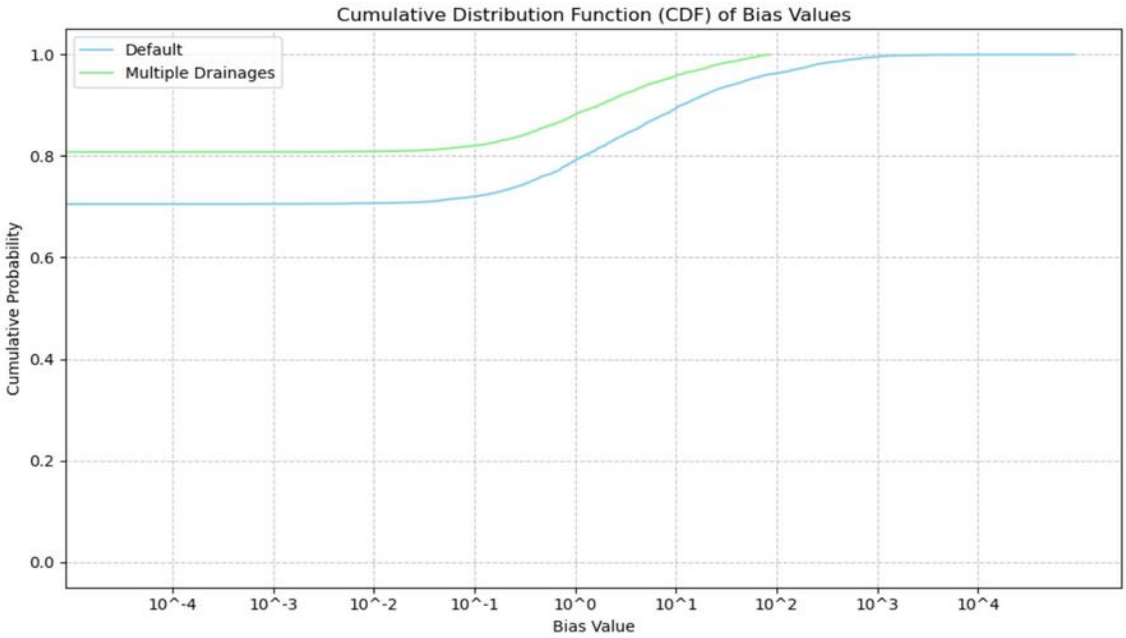
Cumulative Distribution Function (CDF) of Bias Values
Default
Multiple Drainages
Cumulative Probability
1.0
0.8
0.6
0.4
0.2
0.0
10^-4
10^-3
10^-2
10^-1
10^0
10^1
10^2
10^3
10^4
Bias Value

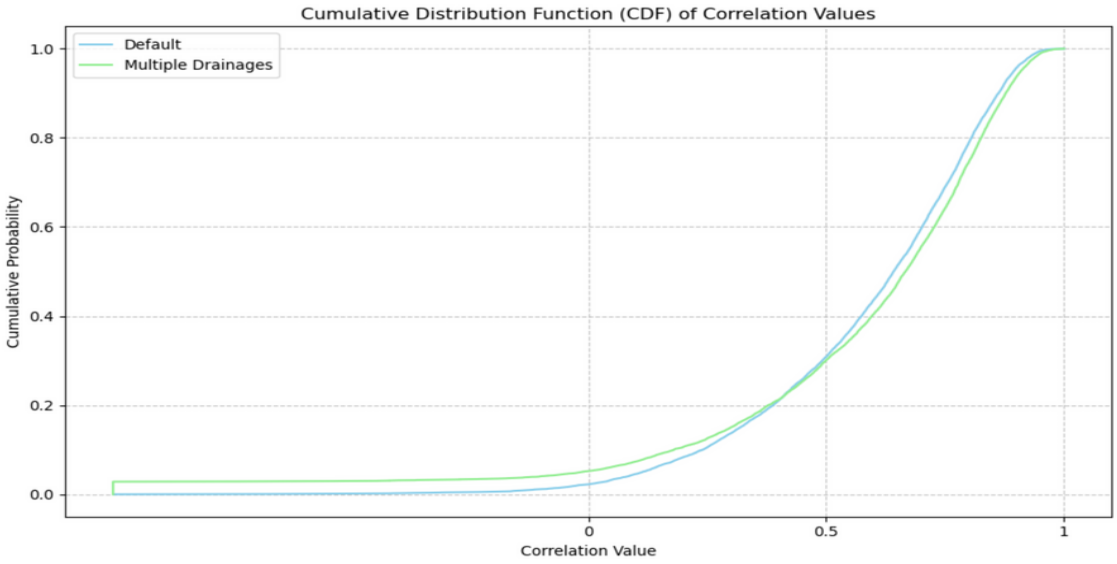

Figure 14 The Cumulation Disribution Function (CDF) curve of variability (top), bias (center), and correlation (bottom) for the multiple drainage model (blue) and default model (green).

4.2.4 Hydrograph

To have a better understanding of the output comparison from the multiple drainages and default model, we choose eight different hydrological stations and plot them (Fig 15). The four first discharges illustrate the area with the better performance of the new model rather than the default model. Fig. 15 depicts the GDRC discharge with the seasonal variability with the different discharge amounts for each location.

The Rio Fresco River in Brazil and the Vienna River in France have a big discharge and peak at 4320 m3/s and 992 m3/s respectively. These two rivers are located in different climatic zones. The first one is located in a tropical rainforest area, with a high precipitation rate and high evaporation rate, while the latter is located in a temperate oceanic climate with medium rainfall and evaporation. Two other hydrograph examples are chosen in the River with a relatively lower discharge. The GRDC discharge at the Crocodile River in South Africa peaks at 445 m3/s, while it has the highest discharge at 57 m3/s for the Goulburn River, Australia. These two areas also have different climate characteristics, the Goulburn River has a tropical monsoon climate with high precipitation and evaporation rate, while the Crocodile River has a semi-arid area with a mid precipitation and high evaporation rate.

This output shows that the improvement in the new model spans various climate characteristics and water flow quantity ranges. These four hydrology areas have similar patterns where the simulated discharge generally underestimates the observation data of GRDC. The area with the best KGE improvement is the Goulburn River, followed by the Rio Fresco River, Vienna River, and Crocodile River. Additionally, the new model captures a temporal dynamic of the discharge well in these four stations, as indicated by a high R-squared value.

On the contrary, the new model performs poorly in some areas. The other four selected hydrology stations illustrate this poor performance. As previously noted, the multiple

drainage model tends to perform worse in dry climates or areas with low precipitation. For example, the Duchesne River in the United States and River Niger in Mali are both locations located in the semi-arid climate. The simulated discharge for the Duchesne River shows a significant underestimated discharge compared to the default and observed GRDC discharge. A unique issue occurs with the Niger River, where the simulated discharge is often zero, failing to capture the monthly discharge pattern.

Furthermore, we plot two other locations with worse results of multiple drainages model performance with different climate characteristics: the Aley River in Russia and the Rhine River in The Netherlands. The Aley River is located in the continental climate with a medium precipitation and evaporation rate. It shows very low simulated discharge and fails to capture the GRDC observation pattern and magnitude as well as the default model. The Rhine River, in a temperate oceanic climate, also experiences underestimated discharge compared to the default model and observed data. The worst KGE changes occur in the Niger River, followed by the Duchesne River, Rhine River, and Aley River.

These four results show that even though there is a general pattern of model improvement or decline, it does not hold for every location. The Crocodile River in South Africa is an example where the arid climate area has a better KGE and R-squared in the new model, while in the Rhine River (Lobith), the performance of the new model has a lower KGE. Specifically for Lobith, despite having a worse KGE, the R-squared of this model shows a better output.

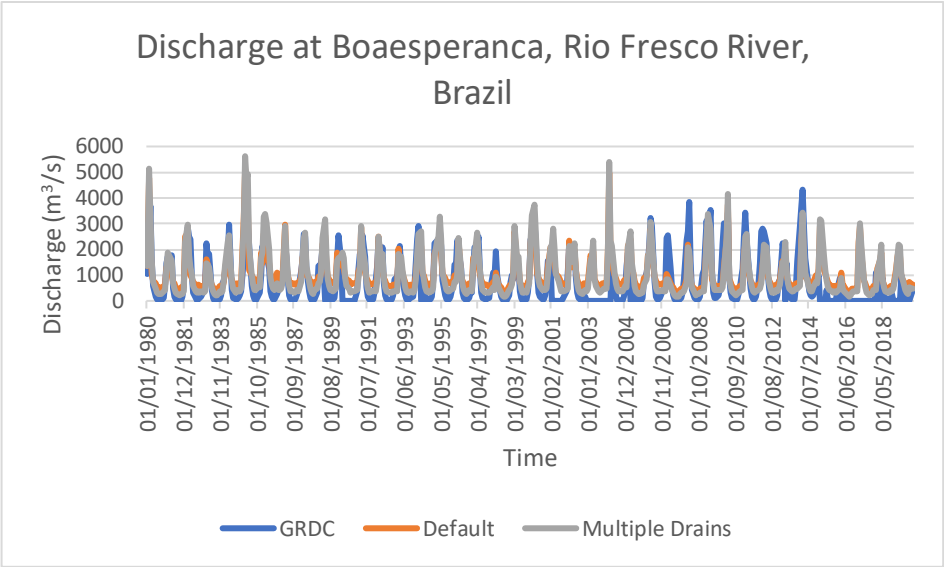
Discharge at Boaesperanca, Rio Fresco River, Brazil
Discharge (m³/s)
6000
5000
4000
3000
2000
1000
0
01/01/1980
01/12/1981
01/11/1983
01/10/1985
01/09/1987
01/08/1989
01/07/1991
01/06/1993
01/05/1995
01/04/1997
01/03/1999
01/02/2001
01/01/2003
01/12/2004
01/11/2006
01/10/2008
01/09/2010
01/08/2012
01/07/2014
01/06/2016
01/05/2018
Time
GRDC
Default
Multiple Drains

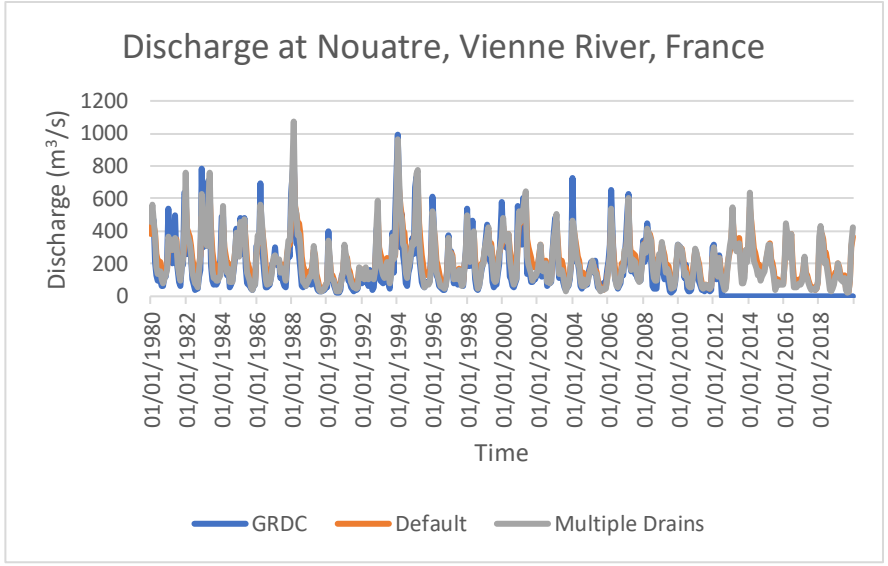
Discharge at Nouatre, Vienne River, France
Discharge (m³/s)
1200
1000
800
600
400
200
0
01/01/1980
01/01/1982
01/01/1984
01/01/1986
01/01/1988
01/01/1990
01/01/1992
01/01/1994
01/01/1996
01/01/1998
01/01/2000
01/01/2002
01/01/2004
01/01/2006
01/01/2008
01/01/2010
01/01/2012
01/01/2014
01/01/2016
01/01/2018
Time
GRDC
Default
Multiple Drains

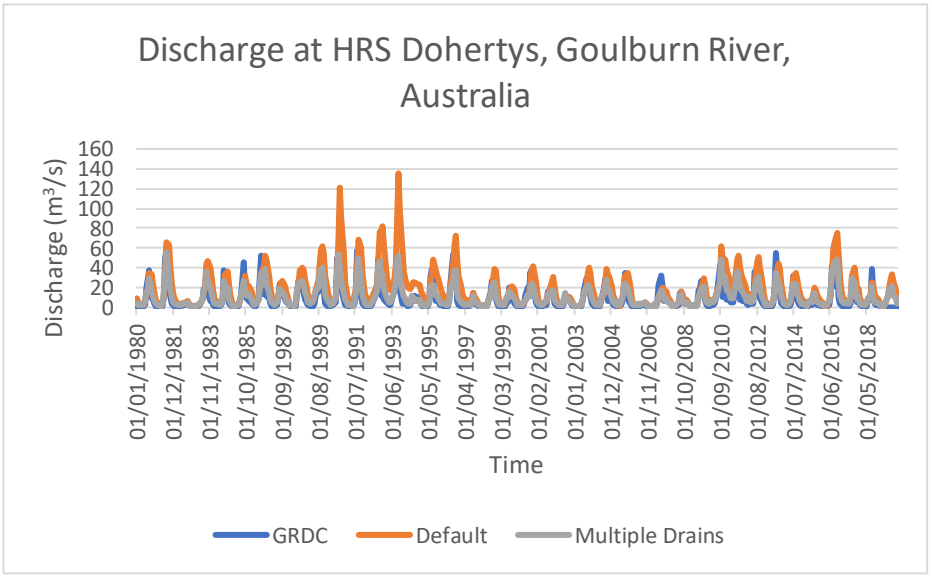
Discharge at HRS Dohertys, Goulburn River, Australia
Discharge (m³/s)
160
140
120
100
80
60
40
20
0
01/01/1980
01/12/1981
01/11/1983
01/10/1985
01/09/1987
01/08/1989
01/07/1991
01/06/1993
01/05/1995
01/04/1997
01/03/1999
01/02/2001
01/01/2003
01/12/2004
01/11/2006
01/10/2008
01/09/2010
01/08/2012
01/07/2014
01/06/2016
01/05/2018
Time
GRDC
Default
Multiple Drains

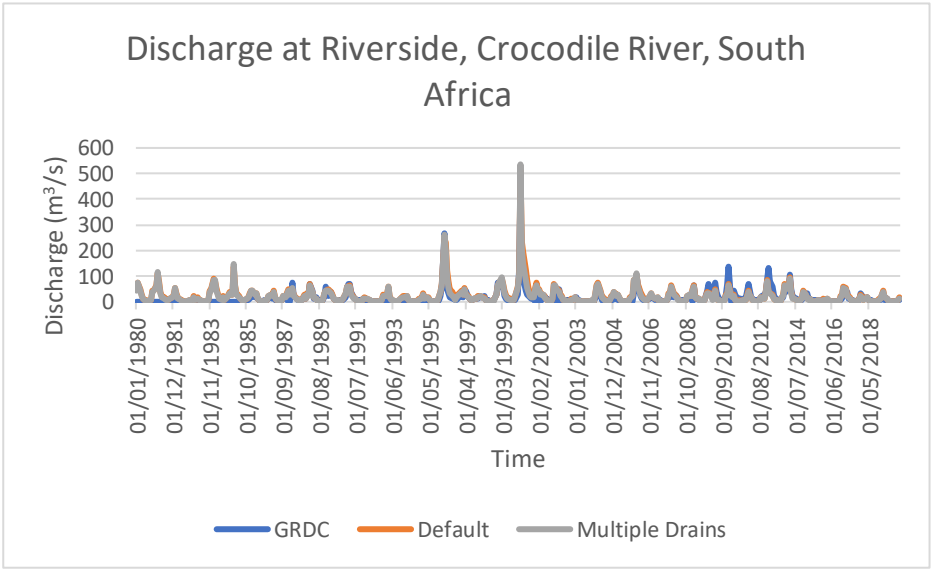
Discharge at Riverside, Crocodile River, South Africa
Discharge (m³/s)
600
500
400
300
200
100
0
01/01/1980
01/12/1981
01/11/1983
01/10/1985
01/09/1987
01/08/1989
01/07/1991
01/06/1993
01/05/1995
01/04/1997
01/03/1999
01/02/2001
01/01/2003
01/12/2004
01/11/2006
01/10/2008
01/09/2010
01/08/2012
01/07/2014
01/06/2016
01/05/2018
Time
GRDC
Default
Multiple Drains

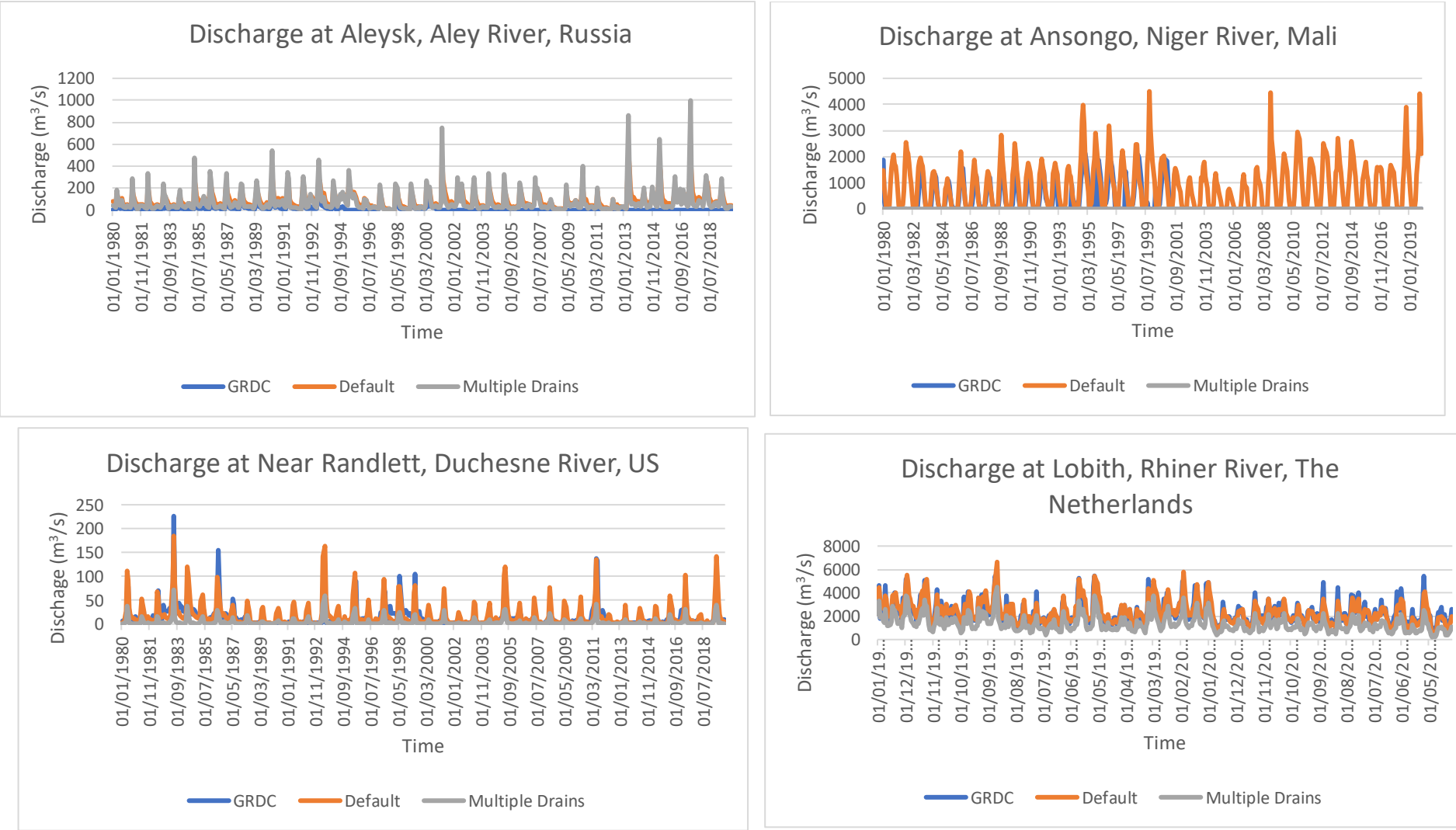

Figure 15 The hydrograph at eight locations of GRDC, default, and new model

5. Discussion

5.1 Evaluation of MODFLOW performance

We simulated the new groundwater model in the test area using MODFLOW 2005 while utilizing MODFLOW 6 on a global scale simulation. In MODFLOW 6, the data can be provided in the unstructured grid, which offers flexibility, especially in complex geological regions, compared to the structural grid in MODFLOW 2005.

The simulation output from this research reveals spatial pattern differences in R-squared, slope, and intercept values between MODFLOW 2005 and MODFLOW 6. For example, in the Rhine-Meuse basin, the R-squared map of the multiple drainages simulation shows a more heterogeneous pattern, whereas the MODFLOW 2005 simulation exhibits a more homogenous and smoother pattern. MODFLOW 6's ability to localize the grid results in more detailed outputs, making differences between values at various points more apparent.

In this study, we did not validate the groundwater head output from MODFLOW 6 to the observation data. However, the validation process could give valuable insight to explain how the new multiple drainages and various conductances concept implementation impact the groundwater head simulation. In future work, the comparison analysis of the groundwater head between this new model and the default model can be conducted.

5.2. The evaluation of parallel simulation

This research failed to simulate the entire region completely. The GLOBGM divides the world into four grid regions, and while three of these regions are perfectly simulated, the last region, representing the island areas, could not be simulated successfully. A technical issue occurred during the 'Partition and Write Model Input' step for the island regions, where one of the cores failed to generate an output file. This failure led to an unsuccessful run in the "Run Mode" step for the island region, rendering the simulation results for island countries and other small islands invalid.

This issue likely arises because some areas, such as Hawaii, are not simulated by PCR-GLOBWB, resulting in missing input data for the simulation. To address this, future research could either improve the PCR-GLOBWB simulation to include these missing areas or fill the missing values with assumed data. A complete simulation covering all regions would provide a more comprehensive overview of the new PCR-GLOBWB model's development and performance.

5.3 Regression analysis

In this study, we deployed a new relationship between baseflow and storage and conducted a regression analysis to determine a new baseflow exponent and recession coefficient parameters as the input of PCR-GLOBWB. Our regression revealed a wide range of the baseflow exponent values, including the area with an excessively high value. Thus, we capped it to the maximum value of 15 to avoid any numerical issues.

At the same time, we obtained significantly lower recession coefficient values compared to the default model. Consequently, the groundwater storage in the model is very stable, making it difficult for water to be released as baseflow. For example, the simulation in Ansongo, Niger River in Mali resulted in zero discharge for most of the time. This location has a very low intercept value and a negative baseflow exponent. It means the increased storage led to more negative baseflow values, indicating that water was infiltrating into storage rather than becoming baseflow. This issue is particularly critical in arid climates where the precipitation rate is low and the discharge is heavily dependent on the baseflow.

Since this current regression approach resulting a very low recession coefficient, a linear regression approach using a new outflow-storage relationship equation could be conducted to improve the model performance, especially to prevent a similar output simulation like at the Niger River occurs. Hence, the utilization of the intercept value from the old model, which is more reliable, is proposed to conduct a regression analysis. This method only determines a new slope or baseflow exponent. The following equation can be used for this purpose:

$$\log\left(\frac{Q}{S_{average}\ x\ \alpha}\right) = \gamma \text{ x} \log(\frac{S}{S_{average}})$$

In this new regression approach, we will plot $\log\left(\frac{Q}{S_{average}\ x\ \alpha}\right)$ as a y-axis, and $\log(\frac{S}{S_{average}})$ as the x-axis. This will yield a new slope or baseflow exponent, potentially providing improved parameter inputs for the PCR-GLOBWB 2 simulation.

6. Conclusion

This research has successfully integrated the multiple drainages and various conductance concepts into the MODFLOW drainage packages and simulated it on a global scale at 30'' resolution using GLOBGM. The implementation of a new relationship between baseflow and groundwater storage captured the non-linear relationship between baseflow and groundwater storage for some grids, as seen in Fig. 7 which shows a varied baseflow exponent.

The performance of PCRGLOBWB 2 in simulating discharge has shown partial improvement. Overall, the model exhibits enhanced performance in regions with high precipitation rates. Conversely, it shows a poorer performance in semi-arid to arid climate areas. Additionally, the new model captures better temporal dynamics, reflected by the improvement in the correlation of the KGE metrics.

References

Chapman, T. (1999). A comparison of algorithms for stream flow recession and baseflow separation. *Hydrological Processes*, *13*(5), 701–714. https://doi.org/10.1002/(sici)1099-1085(19990415)13:5%3C701::aid-hyp774%3E3.0.co;2-2

Condon, L. E., Kollet, S., Bierkens, M. F. P., Fogg, G. E., Maxwell, R. M., Hill, M. C., Fransen, H. H., Verhoef, A., Van Loon, A. F., Sulis, M., & Abesser, C. (2021). Global Groundwater Modeling and Monitoring: Opportunities and Challenges. *Water Resources Research*, *57*(12). https://doi.org/10.1029/2020wr029500

de Graaf, I. E. M., Sutanudjaja, E. H., van Beek, L. P. H., & Bierkens, M. F. P. (2015). A high-resolution global-scale groundwater model. *Hydrology and Earth System Sciences*, *19*(2), 823–837. https://doi.org/10.5194/hess-19-823-2015

de Graaf, I. E. M., van Beek, L. P. H., Wada, Y., & Bierkens, M. F. P. (2014). Dynamic attribution of global water demand to surface water and groundwater resources: Effects of abstractions and return flows on river discharges. *Advances in Water Resources*, *64*, 21–33. https://doi.org/10.1016/j.advwatres.2013.12.002

de Graaf, I. E. M., van Beek, R. L. P. H., Gleeson, T., Moosdorf, N., Schmitz, O., Sutanudjaja, E. H., & Bierkens, M. F. P. (2017). A global-scale two-layer transient groundwater model: Development and application to groundwater depletion. *Advances in Water Resources*, *102*, 53–67. https://doi.org/10.1016/j.advwatres.2017.01.011

Fan, Y., Li, H., & Miguez-Macho, G. (2013). Global Patterns of Groundwater Table Depth. *Science*, *339*(6122), 940–943. https://doi.org/10.1126/science.1229881

Galodha, A., Kayithi, N. S., Sharma, D., & Jain, P. (2023). MONITORING GROUNDWATER STORAGE BASINS AND HYDROLOGICAL CHANGES

USING THE GRACE SATELLITE AND SENTINEL-1 FOR THE GANGA RIVER BASIN. *The International Archives of the Photogrammetry, Remote Sensing and Spatial Information Sciences*, *XLVIII-M-3-2023*, 95–100. https://doi.org/10.5194/isprs-archives-xlviii-m-3-2023-95-2023

Gan, R., & Luo, Y. (2013). Using the nonlinear aquifer storage–discharge relationship to simulate the base flow of glacier- and snowmelt-dominated basins in northwest China. *Hydrology and Earth System Sciences*, *17*(9), 3577–3586. https://doi.org/10.5194/hess-17-3577-2013

Gupta, H. V., Kling, H., Yilmaz, K. K., & Martinez, G. F. (2009). Decomposition of the mean squared error and NSE performance criteria: Implications for improving hydrological modelling. *Journal of Hydrology*, *377*(1-2), 80–91. https://doi.org/10.1016/j.jhydrol.2009.08.003

Harbaugh, A., Banta, E., Hill, M., & Mcdonald, M. (2000). MODFLOW-2000, THE U.S. GEOLOGICAL SURVEY MODULAR GROUND-WATER MODEL-USER GUIDE TO MODULARIZATION CONCEPTS AND THE GROUND-WATER FLOW PROCESS. In *Geological Survey*. CO 4 McDonald Morrissey Associates. https://inside.mines.edu/~epoeter/583CSM/DOC3_MODFLOW2000_ModConcepts_GWFlowProcess_ofr00-92.pdf

Jing, M., Heße, F., Kumar, R., Wang, W., Fischer, T., Walther, M., Zink, M., Zech, A., Samaniego, L., Kolditz, O., & Attinger, S. (2018). Improved regional-scale groundwater representation by the coupling of the mesoscale Hydrologic Model (mHM v5.7) to the groundwater model OpenGeoSys (OGS). *Geoscientific Model Development*, *11*(5), 1989–2007. https://doi.org/10.5194/gmd-11-1989-2018

Knoben, W. J. M., Freer, J. E., & Woods, R. A. (2019). Technical note: Inherent benchmark or not? Comparing Nash-Sutcliffe and Kling-Gupta efficiency scores. *Hydrology and Earth System Sciences Discussions*, 1–7. https://doi.org/10.5194/hess-2019-327

Leur, D. A. K. van de. (1958). A study of non-steady groundwater flow with special reference to a reservoir coefficient. *De Ingenieur*, *70*(19), B87–B94. https://research.wur.nl/en/publications/a-study-of-non-steady-groundwater-flow-with-special-reference-to-

Li, B., Rodell, M., Kumar, S., Beaudoing, H. K., Getirana, A., Zaitchik, B. F., Goncalves, L. G., Cossetin, C., Bhanja, S., Mukherjee, A., Tian, S., Tangdamrongsub, N., Long, D., Nanteza, J., Lee, J., Policelli, F., Goni, I. B., Daira, D., Bila, M., & Lannoy, G. (2019). Global GRACE Data Assimilation for Groundwater and Drought Monitoring: Advances and Challenges. *Water Resources Research*, *55*(9), 7564–7586. https://doi.org/10.1029/2018wr024618

Mahammad, S., Islam, A., Shit, P. K., Towfiqul Islam, A. R. M., & Alam, E. (2023). Groundwater level dynamics in a subtropical fan delta region and its future prediction using machine learning tools: Sustainable groundwater restoration. *Journal of Hydrology: Regional Studies*, *47*, 101385. https://doi.org/10.1016/j.ejrh.2023.101385

Reinecke, R., Foglia, L., Mehl, S., Trautmann, T., Cáceres, D., & Döll, P. (2018). *Beyond the bucket – Developing a global gradient-based groundwater model (G³M v1.0) for a global hydrological model from scratch*. https://doi.org/10.5194/gmd-2018-120

Reinecke, R., Wachholz, A., Mehl, S., Foglia, L., Niemann, C., & Döll, P. (2020). Importance of Spatial Resolution in Global Groundwater Modeling. *Groundwater*, *58*(3), 363–376. https://doi.org/10.1111/gwat.12996

SURF. (n.d.). *Snellius: the National Supercomputer | SURF.nl*. Www.surf.nl. Retrieved May 6, 2024, from https://www.surf.nl/en/services/snellius-the-national-supercomputer

Sutanudjaja, E. H. (2023, July 31). *HYPFLOWSCI6: HYdrological Projection of Future gLObal Water States with CMIP6*. Public.yoda.uu.nl. https://public.yoda.uu.nl/geo/UU01/YM7A5H.html

Sutanudjaja, E. H., van Beek, L. P. H., de Jong, S. M., van Geer, F. C., & Bierkens, M. F. P. (2011). Large-scale groundwater modeling using global datasets: a test case for the Rhine-Meuse basin. *Hydrology and Earth System Sciences*, *15*(9), 2913–2935. https://doi.org/10.5194/hess-15-2913-2011

Sutanudjaja, E. H., van Beek, L. P. H., de Jong, S. M., van Geer, F. C., & Bierkens, M. F. P. (2014). Calibrating a large-extent high-resolution coupled groundwater-land surface model using soil moisture and discharge data. *Water Resources Research*, *50*(1), 687–705. https://doi.org/10.1002/2013wr013807

Sutanudjaja, E. H., van Beek, R., Wanders, N., Wada, Y., Bosmans, J. H. C., Drost, N., van der Ent, R. J., de Graaf, I. E. M., Hoch, J. M., de Jong, K., Karssenberg, D., López López, P., Peßenteiner, S., Schmitz, O., Straatsma, M. W., Vannametee, E., Wisser, D., & Bierkens, M. F. P. (2018). PCR-GLOBWB 2: a 5 arcmin global hydrological and water resources model. *Geoscientific Model Development*, *11*(6), 2429–2453. https://doi.org/10.5194/gmd-11-2429-2018

Van Beek, L. P. H., & Bierkens, M. (2009). *The Global Hydrological Model PCR-GLOBWB: Conceptualization, Parameterization and Verification Report*.

Verkaik, J., Sutanudjaja, E. H., Oude Essink, G. H. P., Lin, H. X., & Bierkens, M. F. P. (2024). GLOBGM v1.0: a parallel implementation of a 30 arcsec PCR-GLOBWB-MODFLOW global-scale groundwater model. *Geoscientific Model Development*, *17*(1), 275–300. https://doi.org/10.5194/gmd-17-275-2024